Targeting the glycan epitope type I *N*-acetyllactosamine enables immunodepletion of human pluripotent stem cells from early differentiated cells

Charlotte Rossdam,[1] Smilla Brand,[1] Julia Beimdiek,[1] Astrid Oberbeck,[1] Marco Darius Albers,[1] Ortwin Naujok,[1] and Falk F. R. Buettner[1,*]

[1]Institute of Clinical Biochemistry, Hannover Medical School, 30625 Hannover, Germany

*Correspondence: buettner.falk@mh-hannover.de (F.F.R.B.)

Abstract

Cell surface biomarkers are fundamental for specific characterization of human pluripotent stem cells (hPSCs). Importantly, they can be applied for hPSC enrichment and/or purification but also to remove potentially teratoma-forming hPSCs from differentiated populations before clinical application. Several specific markers for hPSCs are glycoconjugates comprising the glycosphingolipid (GSL)-based glycans SSEA-3 and SSEA-4. We applied an analytical approach based on multiplexed capillary gel electrophoresis coupled to laser-induced fluorescence detection to quantitatively assess the GSL glycome of human embryonic stem cells and human induced pluripotent stem cells as well as during early stages of differentiation into mesoderm, endoderm, and ectoderm. Thereby, we identified the GSL lacto-*N*-tetraosylceramide (Lc4-Cer, Galβ1-3GlcNAcβ1-3Galβ1-4Glc-Cer), which comprises a terminal type 1 LacNAc (T1LN) structure (Galβ1-3GlcNAc), to be rapidly decreased upon onset of differentiation. Using a specific antibody, we could confirm a decline of T1LN-terminating glycans during the first four days of differentiation by live-cell staining and subsequent flow cytometry. We could further separate T1LN-positive and T1LN-negative cells out of a mixed population of pluripotent and differentiated cells by magnetic activated cell sorting. Notably, not only the T1LN-positive but also the T1LN-negative population was positive for SSEA-3, SSEA-4, and SSEA-5 while expression of nuclear pluripotency markers *OCT4* and *NANOG* was highly reduced in the T1LN-negative population, exclusively. Our findings suggest T1LN as a pluripotent stem cell-specific glycan epitope that is more rapidly down-regulated upon differentiation than SSEA-3, SSEA-4, and SSEA-5.

31 # Introduction

32 Human pluripotent stem cells (hPSCs) including both, human embryonic stem cells (hESCs)
33 as well as human induced pluripotent stem cells (hiPSCs), offer great potential in regenerative
34 medicine as an unlimited cell source that can be differentiated into nearly every somatic cell
35 type (Okano and Yamanaka, 2014; Pera and Trounson, 2004). hPSC-specific cell surface
36 markers are highly relevant for example to define pluripotency and purity of cultured cells.
37 Furthermore, pluripotency-specific markers can be applied for killing or removal of hPSCs from
38 differentiated populations since potentially tumorigenic pluripotent cells present a major hurdle
39 for clinical application of hPSC-derived somatic cells (Fong et al., 2010).

40 Numerous routinely used targets for characterization of hPSCs are cell surface exposed
41 glycoconjugates (Wright and Andrews, 2009) such as the structures detected by the
42 monoclonal antibodies Tra-1-60 and Tra-1-81 that have been shown to recognize a
43 tetrasaccharide epitope which is part of a mucin-type *O*-glycan in hESCs (Natunen et al.,
44 2011). Furthermore, glycosphingolipids (GSLs) belonging to the globo-series (Gb) such as
45 globopentaosylceramide (Gb5-Cer, SSEA-3), sialyl-globopentaosylceramide (sialyl-Gb5-Cer,
46 SSEA-4) (Kannagi et al., 1983), and fucosyl-globopentaosylceramide (fucosyl-Gb5-Cer, Globo
47 H) (Barone et al., 2013) or to the lacto-series (Lc) such as fucosyl-lactotetraosylceramide
48 (fucosyl-Lc4-Cer, Fuc1-2Galβ1-3GlcNAcβ1-3Galβ1-4Glc-Cer) (Liang et al., 2010; Liang et al.,
49 2011) or sialyl-lactotetraosylceramide (Sia-Lc4-Cer, Siaα2-3Galβ1-3GlcNAcβ1-3Galβ1-4Glc-
50 Cer) (Barone et al., 2014) were described to be highly specific for hPSCs and rapidly disappear
51 from the cell surface upon differentiation.

52 Liang *et al.* described a general switch of the core structures of GSLs from globo- and lacto-
53 to ganglio-series upon hPSC differentiation. This switch was accompanied by changes in
54 expression levels of the involved glycosyltransferases (Liang et al., 2010; Liang et al., 2011).
55 Both, globo- and lacto-series GSLs are characterized by a galactose bound in β1-3-linkage to
56 either *N*-acetylgalactosamine (Galβ1-3GalNAc) or *N*-acetylglucosamine (Galβ1-3GlcNAc),
57 respectively. The Galβ1,3GlcNAc disaccharide, which is commonly referred to as type 1

58 LacNAc chain (T1LN) has been found on hPSC-specific *O*-glycans, where it is part of the Tra-
59 1-60 and Tra-1-81 epitopes (Natunen et al., 2011), as well as on *N*-glycans (Hasehira et al.,
60 2012; Konze et al., 2017). Appearance of these structures is likely associated with the hPSC-
61 specific expression of the major β1,3-galactosyltransferase (B3GALT5) (Tateno et al., 2011).

62 By screening of antibody libraries, an hPSC-specific antibody targeting the glycan structure
63 Fuc1-2Galβ1-3GlcNAcβ, which is designated as H type-1 (H-1), was found. The H-1 epitope
64 also contains a T1LN motif. This H-1-epitope-specific antibody, termed SSEA-5, was shown
65 to detect protein *N*- and *O*-glycans (Tang et al., 2011). The H-1 epitope is also part of the
66 lactoseries GSL fucosyl-Lc4-Cer whose levels considerably decline upon differentiation of
67 hPSCs into embryoid bodies (EBs) (Liang et al., 2010). Tang *et al.*, demonstrated the potential
68 of the H-1 epitope to be immunologically targeted for prospective removal of hPSCs from mixed
69 populations. hPSCs that were spiked into a population of hPSC-derived, fully differentiated
70 cells could be efficiently removed by fluorescence-activated cell sorting (FACS) using the
71 SSEA-5 antibody. This completely abolished teratoma-formation potential of the SSEA-5-
72 immunodepleted population. However, applying the same sorting strategy for a pure
73 population of day-3 differentiated hPSCs gave rise to an immunodepleted population which
74 still caused teratoma formation. It was necessary to target two additional hPSC-specific cell
75 surface proteins to finally select for cells that did not cause teratoma (Tang et al., 2011). These
76 findings show that, until now, individual markers like H-1 are not sufficient for complete
77 separation of hPSCs from early differentiated progeny, pointing towards the necessity for the
78 identification of additional hPSC-specific cell surface markers.

79 We have established multiplexed capillary gel electrophoresis coupled to laser-induced
80 fluorescence detection (xCGE-LIF) as a powerful technique for the analysis of GSL
81 glycosylation (Cumin et al., 2022; Jirmo et al., 2020; Rossdam et al., 2019; Starzonek et al.,
82 2020) and used this approach to screen for hPSC markers. A quantitative comparison of GSL
83 glycan levels in hPSCs (hESCs and hiPSCs) and upon early lineage-specific differentiation
84 revealed the lactoseries GSL lacto-*N*-tetraosylceramide (Lc4-Cer, Galβ1-3GlcNAcβ1-3Galβ1-

85 4Glc) to be significantly down-regulated in hPSCs upon differentiation. Lc4-Cer contains a
86 T1LN motif and by applying a T1LN-specific antibody, we confirmed surface expression of
87 T1LN-containing glycans by flow cytometry. Using this antibody for magnetic activated cell
88 sorting (MACS), we could quantitatively separate T1LN-expressing hPSCs from early
89 differentiated cells. The comparison of T1LN glycans to other well-known hPSC surface
90 markers, such as SSEA-3, SSEA-4 or H-1 corroborated the suitability of T1LN as a superior
91 marker for undifferentiated hPSCs.

92

93 **Results**

94 xCGE-LIF-based profiling of GSL glycosylation reveals Lc4-Cer as a
95 hPSC marker

96 We applied xCGE-LIF to analyze GSL glycosylation of hPSCs (hESCs and hiPSCs) and during
97 early stages of differentiation with the aim to identify potential novel GSL-based biomarkers of
98 hPSCs. Therefore, we differentiated both cell lines for 4 days into early stages of mesoderm,
99 endoderm, and ectoderm and confirmed successful lineage specification on day 4 of
100 differentiation (d4) by flow cytometric analyses of lineage-specific differentiation markers
101 (Suppl. Figure S1). Differentiation into mesoderm resulted in the characteristic balanced cell
102 surface expression of the adhesion molecules NCAM and EpCAM as described by Kempf *et*
103 *al.* (Kempf et al., 2016b). Endodermal differentiation resulted in 87±5 % and 85±6 % CXCR4
104 positive hES-derived and hiPS-derived cells, respectively. For ectoderm, we observed 95±2 %
105 and 97±1 % Pax-6-positive hES-derived and hiPS-derived cells, respectively (Suppl. Figure
106 S1). For both cell lines and all differentiation approaches we harvested cells on day (d)0, d1,
107 d2, d3, and d4 and analyzed GSL glycosylation by xCGE-LIF (Figure 1). This analysis revealed
108 down-regulation of the known pluripotency-associated GSLs SSEA-3, SSEA-4, and fucosyl-
109 Lc4-Cer (containing the terminal H-1 trisaccharide epitope Fuc1-2-Galβ1-3GlcNAcβ, detected
110 by the SSEA-5 antibody) and/or globo H upon differentiation into the three germ layers.
111 Notably, the GSLs fucosyl-Lc4-Cer (comprising the H-1 epitope) and globo H could not be

112 discriminated as they comigrated in the capillary gel electrophoresis. However, using
113 exoglycosidase digestions, we confirmed that the respective signal arises from both structures
114 (data not shown). In addition to these rather expected findings, we identified the GSL glycan
115 lactotetraose (Lc4) to be down-regulated during differentiation. Especially upon mesodermal
116 and endodermal differentiation the decline of Lc4-levels was stronger than for the known
117 marker structures. For ectodermal differentiation, we did not observe down-regulation of Lc4-
118 levels. However, also the known markers showed a heterogenous profile depending on the
119 analyzed cell line.
120

121 Cell surface levels of T1LN strongly decline after four days of hPSC 122 differentiation

123 As a complementary approach, we analyzed non-permeabilized hPSCs (d0) as well as their
124 progeny on d4 of differentiation into meso-, endo-, and ectoderm by flow cytometry applying
125 the BG-1 antibody detecting a terminal T1LN-structure (Domino et al., 2001) as present in Lc4-
126 Cer (Figure 2, Suppl. Figure S3). The differentiation outcome was scrutinized by analysis and
127 quantification of marker expression as described above (Suppl. Figure S2). The flow cytometric
128 analyses revealed a strong and significant decline of T1LN cell surface levels upon
129 differentiation for 4 days into all three lineages for both hESCs and hiPSCs (Figure 2 A, B left
130 panels). We also assessed cell surface expression of SSEA-4 and H-1 (SSEA-5) by flow
131 cytometry using specific antibodies. We observed a mild to moderate decrease of cell surface
132 levels of these known markers upon differentiation. Notably, SSEA-4 and H-1 down-regulation
133 was for all germ layers less pronounced than down-regulation of T1LN (Figure 2 A, B middle
134 and right panels). Taken together, our findings strongly suggest T1LN as a highly specific cell
135 surface marker for undifferentiated hPSCs that is characterized by rapid down-regulation upon
136 differentiation.

137

T1LN-expressing cells could be efficiently depleted by magnetic cell sorting from mixed populations

Cell surface markers enabling the immunological identification and prospective depletion of hPSCs, such as SSEA-5 described by Tang and colleagues (Tang et al., 2011), are highly demanded in regenerative medicine, since residual contaminating hPSCs within differentiation cultures might cause the formation of teratoma or teratocarcinoma upon transplantation into human recipients. With the aim to scrutinize whether the T1LN glycan epitope is useful in the above described setting, we again differentiated hPSCs (hESCs and hiPSCs) for 4 days into early meso-, endo-, and ectoderm and confirmed successful differentiation for both cell lines into all germ layer differentiations (Suppl. Figure S4). We repeated the flow cytometric analyses of d0 and d4 cells for T1LN, SSEA-4, H-1 (SSEA-5), and additionally analyzed SSEA-3 surface expression (Figure 3B). This analysis basically mirrored our previous findings (Figure 2) that the expression of T1LN as well as of known hPSC surface markers was significantly reduced on d4 of differentiation (Figure 3B, Suppl. Figure S5). To further evaluate whether hPSCs could be depleted from mixed populations based on their T1LN expression, we pooled equal cell numbers of hPSCs (hESCs or hiPSCs, d0) and their mesodermal, endodermal or ectodermal derivatives (d4, Figure 3A). Flow cytometric analyses of surface markers of the pooled population (d0/d4-pool) mostly revealed, as expected, intermediate values for fluorescence intensities (Figure 3B, Suppl. Figure S5). Using magnetic microbeads decorated with the T1LN-specific BG-1 antibody for MACS analyses, we could obtain an unbound fraction with less than 1% of cells being detected as T1LN-positive by subsequent flow cytometry (Figure 3B, Suppl. Figure S5). This fraction was designated as T1LN-negative and confirmed the successful depletion of T1LN-positive cells from the mixed population. Notably, expression of the stem cell markers SSEA-4 and H-1 (SSEA-5), were - if at all - only slightly reduced in the unbound T1LN-negative fraction in comparison to the d0/d4-pool. On the other hand, levels of SSEA-3 and T1LN were significantly diminished (Figure 3B, Suppl. Figure S6). All analysed surface markers were detected at high levels upon MACS in the bound fraction, which we designated as T1LN-positive. Taken together, our analyses revealed that upon germ layer

166 differentiation a substantial fraction of cells already had lost T1LN cell surface expression while
167 still carrying the pluripotency markers SSEA-3, SSEA-4, and H-1 (SSEA-5) on their cell surface
168 (Suppl. Figure S6).

169

170 Expression of *OCT4* and *NANOG* is strongly reduced in the T1LN-
171 negative population

172 The transcription factors OCT4 and NANOG are generally considered as gold standards for
173 pluripotency of hPSCs. We therefore assessed their gene expression by quantitative PCR
174 (qPCR) in the different populations comprising hPSCs (d0), differentiated cells (d4), pooled
175 cells (d0/d4-pool), and upon MACS of the sorted cells (T1LN-pos and T1LN-neg). This analysis
176 expectedly revealed high expression of *OCT4* and *NANOG* in d0 hPSCs which was drastically
177 diminished upon 4 days of differentiation (d4) for both cell lines and all differentiation
178 approaches (Figure 3C). The d0/d4-pool showed an expected intermediate expression of
179 *OCT4* and *NANOG*. Upon cell sorting by MACS, we observed high expression of these
180 markers in the T1LN-positive population and a strongly reduced expression in the T1LN-
181 negative population which was even lower than on d4. This finding suggests that the T1LN-
182 negative population is highly depleted of pluripotent cells. As we previously showed that the
183 T1LN-negative population is still positive for SSEA-3, SSEA-4, and H-1 (SSEA-5), T1LN
184 seems to be a more sensitive cell surface pluripotency maker than the other commonly applied
185 glycan markers.

186

187 T1LN cell surface levels are correlated to *B3GALT5* gene expression

188 The cell surface glycan epitopes T1LN, SSEA-3, SSEA-4, and H-1 (SSEA-5) all contain a
189 galactose bound in β1-3-linkage to either GlcNAc or GalNAc which is synthesized by the
190 enzyme B3GALT5 (Zhou et al., 2000). Thus, we also determined *B3GALT5* expression by
191 qPCR in our pre- and post-MACS cell populations (d0, d4, d0/d4-pool, T1LN-pos, T1LN-neg).

192 Thereby a decrease of *B3GALT5* mRNA expression on d4 vs. d0 for both cell lines and
193 mesodermal, endodermal, and ectodermal differentiations was observed. *B3GALT5*
194 expression appeared to be even more strongly reduced in the post-MACS T1LN-neg cell
195 population than on d4 of differentiation hinting towards a strong correlation of T1LN levels and
196 *B3GALT5* expression. (Figure 3C).

197

198 ## Discussion

199 Ideal surface markers for hPSCs correlate with the pluripotent state and can be efferently
200 targeted by specific antibodies. Thereby such markers can be applied to examine pluripotency
201 but also for antibody-based enrichment or depletion of hPSCs. In particular, immunodepletion
202 of hPSCs from *in vitro* differentiated populations has gained attention as residual hPSCs might
203 give rise to teratoma formation upon clinical application in human (Fong et al., 2010).
204 Strategies for depletion of hPSCs for example comprise specific cytotoxic antibodies (Choo et
205 al., 2008; Tan et al., 2009), prospective removal by fluorescence-activated cell sorting (Tang
206 et al., 2011) and suicide gene-mediated ablation of pluripotent cells (Naujok et al., 2010). To
207 prevent teratoma formation in mice, a combination of different cell surface markers was
208 necessary for comprehensive immunodepletion of hPSCs from early differentiated populations
209 (Tang et al., 2011), highlighting the need to search for further highly specific hPSC markers.

210 Many widely applied cell surface markers for hPSC characterization are glycoconjugates such
211 as the *O*-glycan epitopes Tra-1-60 and Tra-1-81 (Natunen et al., 2011) or the globoseries GSLs
212 SSEA-3 and SSEA-4 which were long known cell surface markers of stem cells and
213 teratocarcinoma cells (Carpenter et al., 2004; Kannagi et al., 1983). Furthermore, the glycan
214 epitope sialyl-Lc4 was shown to be present on glycoproteins and GSLs of hPSCs and this
215 glycan structure rapidly decreased upon differentiation into hepatocyte- and cardiomyocyte-
216 like cells (Barone et al., 2014). Additionally, the H-1 epitope which can build the terminal
217 structure of *O*-glycans, *N*-glycans and GSL-glycans (e.g. Fuc-Lc4-Cer) was discovered by

218 Liang *et al.* to be down-regulated upon hPSC differentiation (Liang et al., 2010). Shortly after,
219 Tang *et al*. introduced the hPSC-specific anti-SSEA-5 antibody directed against the H-1 glycan
220 epitope and well suited for immunodepletion of hPSCs from mixed cell populations (Tang et
221 al., 2011).

222 GSLs comprise a highly diverse family of glycosylated membrane constituents whose
223 synthesis is tightly controlled by the cellular state and during cell fate specification, rendering
224 them attractive marker candidates (D'Angelo et al., 2013; Russo et al., 2018). When we
225 recently profiled changes in GSL glycosylation upon cardiomyogenic differentiation of hPSCs,
226 we not only noted strongly reduced levels of the known markers SSEA-3, SSEA-4, globo H,
227 and Fuc-Lc4-Cer (comprising the H-1 epitope which can be detected by the anti-SSEA5
228 antibody), but also of its biosynthetic precursor Lc4-Cer (Rossdam et al., 2019). Therefore, we
229 assessed GSL glycosylation of hPSCs and during early stages of lineage-specific
230 differentiation applying our novel xCGE-LIF-based analytical approach. This analysis revealed
231 that Lc4-Cer levels rapidly decline upon differentiation. In 2010, Liang *et al.* first described Lc4-
232 Cer to be down-regulated upon hESC differentiation into embryoid bodies. However, in latter
233 and subsequent studies, Lc4-Cer could not be clearly distinguished from its structural isomers
234 Gb4-Cer (GalNAcβ1-3Galα1-4Galβ1-4Glc-Cer) and nLc4 (Galβ1-4GlcNAcβ1-3Galβ1-4Glc) by
235 using MALDI-MS, MALDI-MS/MS or LC-MS/MS for glycosphingolipid profiling (Fujitani et al.,
236 2013; Ho et al., 2017; Liang et al., 2010; Liang et al., 2011; Lin et al., 2020; Ojima et al., 2015).
237 However, our xCGE-LIF-based approach clearly distinguished Lc4 from its structural isomer
238 Gb4 and even its linkage isomer nLc4 (Rossdam et al., 2019). In accordance to our
239 observations, Lc4-Cer could be unambiguously detected from hESC- and hiPSC-derived GSLs
240 by capillary liquid chromatography-based separation of structural isomers of
241 tetraglycosylceramides and subsequent ESI/MS as well as by NMR analysis (Barone et al.,
242 2013; Säljö et al., 2017), but these studies did not assess the effect of hPSC differentiation on
243 Lc4-Cer levels.

244 We additionally performed flow cytometry using the BG-1 antibody specific for the T1LN
245 structure (Domino et al., 2001) present in Lc4-Cer. To the best of our knowledge there is no
246 antibody available which exclusively binds to Lc4-Cer. BG-1 will also detect *N*- and *O*-glycans
247 containing the T1LN epitope which has been previously reported to be hPSC-specific by us
248 and others (Hasehira et al., 2012; Konze et al., 2017; Natunen et al., 2011). Our flow cytometric
249 analyses showed that the cell surface reactivity towards the BG-1 antibody strongly declined
250 during differentiation, suggesting that not only Lc4-Cer but also levels of *N*- and *O*-glycans
251 carrying T1LN structures decreased. Probably using the same antibody as we did (both are
252 designated as clone K21), Liang *et al.* performed flow cytometry analyses and claimed a
253 significant down-regulation of Lc4-Cer on hESCs upon differentiation into neural progenitor
254 cells and definitive endoderm (Liang et al., 2011). However, according to the specificity of this
255 antibody, they most likely also detected a decline of T1LN structures, irrespective to which type
256 of glycan they belong to. Anyhow, while Liang *et al.* analyzed the cells after 2-3 weeks of
257 differentiation, we differentiated the hESCs and hiPSCs for only 4 days into all three germ
258 layers and thereby could show that T1LN already decreases in early stages of differentiation.

259 The β-1-3-specific transfer of galactose to either *N*-acetylglucosamine giving rise to T1LN
260 structures (as present in the H-1 epitope detected by the SSEA-5 antibody or in Lc4-Cer) or to
261 *N*-acetylgalactosamine as present in globoseries GSLs (e.g. SSEA-3, SSEA-4, globo H) is
262 catalyzed by the enzyme β-1-3 galactosyltransferase (B3GALT5, (Zhou et al., 2000)). We
263 noted in our study that differentiation is accompanied by rapid downregulation of *B3GALT5*
264 expression. This finding is in accordance with previous studies showing a significant
265 downregulation of *B3GALT5* gene expression upon hPSC differentiation (Liang et al., 2010;
266 Liang et al., 2011; Ojima et al., 2015). Down-regulation of *B3GALT5* gene expression is likely
267 to be associated with reduced synthesis of glycans containing β-1-3-linked galactose
268 comprising glycans with T1LN structures. Interestingly, we observed that cell surface levels of
269 glycans with terminal T1LN-structures decreased more rapidly upon differentiation than those
270 of their fucosylated downstream products harboring a H-1 epitope (detected by the SSEA-5
271 antibody). Strikingly, the sorted T1LN-negative population on day 4 of differentiation still

272 contained significant levels of glycans detected by the SSEA-5 antibody. In analogy to our
273 findings, it was previously shown that hESCs or human embryonal carcinoma cells lose SSEA-
274 3 expression before they lose expression of its biosynthetic product sialyl-SSEA-3 (SSEA-4)
275 (Draper et al., 2002; Fenderson et al., 1987; Wright and Andrews, 2009). Based on these
276 findings, we hypothesize that differentiation-induced down-regulation of *B3GALT5* will lead to
277 a reduced synthesis of T1LN structures while existing T1LN structures are still further
278 converted into their downstream products, e.g. H-1 or SSEA-4 antigens. Thus, during
279 continuous cellular proliferation, levels of glycans with T1LN structures are more rapidly
280 depleted from the cell surface than their biosynthetic products (Figure 4). This hypothesized
281 mechanism can also explain the previously made observations for the SSEA3 and SSEA4
282 couple. Confirmatory to this model, we observed in the T1LN-negative population that SSEA3
283 levels were considerably lower than SSEA4 levels, but where interestingly still higher than
284 T1LN levels. Thus, we claim that T1LN is a superior stem cell marker compared to SSEA-3,
285 SSEA-4, and H-1 (fucosyl-Lc4 detected by the SSEA5 antibody) as it more rapidly declines
286 upon onset of differentiation.

287

288 **Materials and Methods**

289 Human pluripotent stem cell culture

290 Cell culture reagents and cell culture vessels were obtained from Thermo Fisher Scientific
291 (Waltham, MA) and Greiner (Greiner Bio-One, Frickenhausen, Germany), respectively, unless
292 stated otherwise. Both the human embryonic stem cell (hESC) line (ES03: ES Cell
293 International, National Stem Cell Bank Wisconsin, WI; H9: WA09 Wisconsin Alumni Research
294 Foundation (Wicell Research Institute, Inc.) Madison, WI), as well as the human induced
295 pluripotent stem cell (hiPSC) line (HSC_Iso4_ADCF-iPC2 “Phoenix” (Haase et al., 2017;
296 Kempf et al., 2016a) were maintained at 37 °C with 5% CO_2 and 85% relative humidity. Culture
297 of hESCs was conducted under standard conditions on γ-irradiated human fibroblasts (human
298 foreskin fibroblasts CCD919, ATCC, Manassas, VA) (Thiesler et al., 2016) in stem cell medium

299 consisting of KnockOut™ DMEM supplemented with 20% KnockOut™ Serum Replacement,
300 1% (v/v) MEM Nonessential Amino Acids, 0.05% (v/v) GlutaMax™, 0.1 mM 2-mercaptoethanol
301 (all reagents obtained from Life Technologies, Carlsbad, CA) and 50 ng/ml basic fibroblast
302 growth factor (bFGF, Institute of Technical Chemistry, Leibniz University Hannover, Hannover,
303 Germany). For passaging every 7 days, cells were incubated with 0.2% (w/v) Collagenase IV
304 (Life Technologies) for 5-10 min at 37 °C and subsequently transferred onto new feeder cells,
305 which were seeded 24 h prior. For further analysis, hESCs were cultivated at least three
306 passages under feeder-free conditions on Matrigel® (1:60 dilution, Corning, Corning, NY) in E8
307 medium (Chen et al., 2011) to exclude contaminating feeder cells. hiPSCs were routinely
308 cultured under feeder-free conditions as monolayer on Matrigel® in E8 medium (Rossdam et
309 al., 2019). For passaging of both hiPSCs and hESCs every 3-4 days under feeder-free
310 conditions, cells were incubated with 0.5 mM EDTA in PBS for 1 min at room temperature and
311 subsequently reseeded onto new Matrigel®-coated flasks.

312 Differentiation into the three germ layers

313 Differentiation into the three germ layers was performed in suspension culture in Corning®
314 Costar® Ultra-Low Attachment 6-well-plates (Merck, Darmstadt, Germany). Prior to seeding,
315 the cells were singularized using 0.5 mM EDTA in PBS for 10 min at 37 °C. For mesodermal/
316 ectodermal and endodermal differentiation, 3.3 x 10^5 cells and 2.6 x 10^5 cells per ml were
317 seeded in 3 ml E8 medium supplemented with 10 µM Rho-associated coiled-coil kinase
318 (ROCK) inhibitor Y-27632 (RI, STEMCELL Technologies, Vancouver, Canada), respectively.
319 For both mesodermal and ectodermal differentiation, the medium was replaced 48 h after
320 seeding on day -2 and again on day -1 of differentiation by E8 medium without RI
321 supplementation. Mesodermal differentiation was performed as described previously by Kempf
322 *et al.* with minor modifications (Kempf et al., 2016a). Briefly, the differentiation was initiated on
323 d0 by replacing the medium with RPMI/B27™ minus insulin (RPMI 1640 supplemented with
324 1% (v/v) GlutaMax™, 2% (v/v) B27™ minus insulin) supplemented with 13.5 µM CHIR99021
325 (Selleckchem, Houston, TX). The medium was replaced on d1 with RPMI/B27™ minus insulin
326 supplemented with 5 µM IWP-4 (STEMCELL Technologies). On d3 medium change was

327 performed using RPMI/B27™ minus insulin without any supplementation. Ectodermal
328 differentiation was adapted from a protocol previously described by Shi *et al.* (Shi et al., 2012).
329 Briefly, the differentiation was initiated on d0 by replacing the E8 medium with neural induction
330 medium (1:1 mixture of N-2 containing medium (DMEM/F12 medium (PAN Biotech,
331 Aidenbach, Germany) supplemented with 1% (v/v) N-2 (Invitrogen), 5 µg/ml insulin (Merck),
332 1% (v/v) GlutaMax™, 1% (v/v) MEM Nonessential Amino Acids, 0.1 mM 2-mercaptoethanol
333 and B27™ containing medium (Neurobasal medium (Invitrogen) supplemented with 2% (v/v)
334 B27™ minus insulin and 1% (v/v) GlutaMax™) supplemented with SB431542 (10 µM) and
335 Dorsomorphin (1 µM, both STEMCELL Technologies). Medium was replaced daily.
336 Endodermal differentiation was performed as described previously by Diekmann *et al.* with
337 minor modifications (Diekmann et al., 2015). Briefly, differentiation was initiated on d0 24 to 48
338 h after seeding by replacing the medium with RPMI/B27™ minus insulin (RPMI 1640
339 supplemented with 1 % (v/v) GlutaMax™, 1% (v/v) B27™ minus insulin) supplemented with 5
340 µM CHIR99021 and 33.3 ng Activin A (STEMCELL Technologies). Medium was exchanged
341 daily without CHIR99021 supplementation. All differentiations were stopped on d4 of
342 differentiation by harvesting the cells for further analyses.

343 Glycolipid extraction and deglycosylation

344 Glycolipids were extracted from cells as previously described (Rossdam et al., 2019). Briefly,
345 approximately 2 x 10^6 cells were harvested on each day of differentiation and stored at -80 °C
346 until further use. Glycolipids were extracted by homogenizing the cell pellets in 1:2
347 chloroform/methanol (v/v) by sonication. Cell debris and proteins were removed by
348 centrifugation at 1620 x g for 5 min and the extract was transferred into a new glass vessel.
349 To ensure a complete extraction, this step was repeated with 1:1 chloroform/methanol (v/v)
350 and 2:1 chloroform/methanol (v/v), respectively. The pooled extracts were further desalted and
351 purified on a Chromabond® C_{18} ec poplyprolyene column (Macherey-Nagel, Düren, Germany).
352 The extracted glycolipids were evaporated to dryness under nitrogen gas to remove organic
353 solvents for deglycosylation. To release the glycan head groups from glycosphingolipids
354 (GSLs), the extracted glycolipids were digested with the GSL-specific LudgerZyme ceramide

355 glycanase (CGase) from *Hirudo medicinalis* (Ludger Ltd, Abingdon, UK) for 24 h at 37 °C in
356 the provided reaction buffer (Ludger Ltd). Released glycans were fluorescently labeled with 8-
357 aminopyrene-1,3,6-trisulfonic acid (APTS, Merck). Briefly, the glycans were mixed with 2 µl
358 APTS (20 mM in 3.5 M citric acid), the reducing agent 2 µl 2-picoline borane complex (PB, 2
359 M in DMSO, Merck) and 2 µl water. Labeling was achieved by incubation for 16.5 h at 37 °C
360 in the dark. The reaction was stopped by adding 100 µl 80:20 acetonitrile/water (v/v). The
361 labeled glycans were purified by performing a HILIC-SPE as previously described (Rossdam
362 et al., 2019). Briefly, the reaction mixture was applied onto a GHP membrane of a Pall
363 Nanosep® MF Centrifugal Device (pore size 0.45 µm, Merck) loaded with a 100 mg/ml Biogel
364 P-10 Gel (Bio-Rad, Hercules, CA) solution. The excess of APTS and reducing agent were
365 removed by washing the column with 80:20 acetonitrile/water (v/v) supplemented with and
366 without 100 mM trimethylamine (pH 8.5), respectively. Labeled glycans were eluted in water
367 and concentrated in a SpeedVac concentrator and stored at -20 °C until further use.

368 Multiplexed capillary gel electrophoresis coupled to laser-induced 369 fluorescence detection (xCGE-LIF)

370 Unless stated otherwise, xCGE-LIF equipment was purchased from Applied Biosystems™
371 (Thermo Fisher Scientific, Foster City, CA). xCGE-LIF of APTS-labelled glycosphingolipid-
372 derived glycans was carried out as previously described (Rossdam et al., 2019). Briefly, APTS-
373 labelled glycans were prepared for xCGE-LIF in a 1:10 dilution in water (water for
374 chromatography, LC-MS grade, Merck) and mixed with 1 µl GeneScan™ 500 LIZ™ dye Size
375 Standard (1:50 dilution in HiDi™ Formamide) in HiDi™ Formamide in a total volume of 10 µl
376 in a MicroAmp™ Optical 96-Well Reaction Plate. The analysis was carried out for 30 min at 12
377 kV and 60 °C using an ABI PRISM® 3100-*Avant* Genetic Analyzer (remodeled by advanced
378 biolab service GmbH, Munich, Germany) equipped with a 4-Capillary Array of 50 cm length
379 filled with POP-7™ Polymer. Data was further processed using the GeneMapper™ Software
380 v3.7. The migration time range of 10 to 300 MTU of resulting xCGE-LIF electropherograms
381 was further processed using Microsoft Word Excel and GraphPad Prism 5.01 software.

382 Relative signal intensities were calculated for individual peak intensities (heights) in relation to
383 the sum of all peak intensities and displayed as percentage enabling comparison of individual
384 peaks from different samples. The in-house migration time data base (Rossdam et al., 2019)
385 enabled annotation of obtained migration times to the target glycan structures Lc4, SSEA3,
386 SSEA4, and SSEA5. Statistical analyses were performed using GraphPad Prism 5.01 software
387 and *p*-values of <0.05 upon unpaired Student's *t*-test were regarded as statistically significant
388 and displayed.

389 Flow cytometric analysis

390 Cell surface expression of T1LN structures , H-1 structures (detected by the anti-SSEA-5
391 antibody), and globoseries GSLs SSEA-3 and SSEA-4 was analyzed by flow cytometry on d0
392 and d4 of differentiation. For this, the cells were harvested and dissociated into single cells by
393 incubation with Accutase (STEMCELL Technologies) for 10 min at 37 °C. To ensure complete
394 dissociation, cells were filtered through a Pre-Separation Filter (50 µm, Sysmex, Norderstedt,
395 Germany). For Pax-6 staining only, cells were fixed for 20 min at 4 °C with paraformaldehyde
396 (PFA, 4 % (w/v) in PBS) and permeabilized with Tween-20 (0.1 % (v/v) in PBS) for 15 min at
397 4 °C. All cells were pelleted and resuspended in fresh FACS buffer (1 % (w/v) BSA and 1 mM
398 EDTA in PBS) and approximately 3 x 10^5 cells were incubated with the respective antibody or
399 the isotype control for 20 min at 4 °C in dilutions as listed in Table S1. After antibody staining,
400 the cells were washed and resuspended in FACS buffer and analyzed using a CyFlow ML flow
401 cytometer (Sysmex Partec, Görlitz, Germany). The data were processed using FlowJo v7.6.4
402 software. Differentiation and stem cell marker expression was analyzed in the gated population
403 of viable cells (determined in an unstained control of both d0 and d4). For quantification of cells
404 positive for their respective differentiation marker, cells which showed intensities higher than
405 99% of the respective isotype control were regarded as positive for the respective marker. For
406 quantification of cells positive for T1LN, SSEA-4, and H1- structures (SSEA-5) the mean
407 fluorescence intensity (MFI) of the respective target was determined and subtracted from the
408 MFI of the respective isotype control. Statistical analyses were performed using GraphPad

409 Prism 5.01 software and *p*-values of <0.05 upon unpaired Student's *t*-test were regarded as
410 statistically significant.

411 Magnetic activated cell sorting

412 To remove T1LN-positive cells from a mixed population, magnetic activated cell sorting
413 (MACS) was applied using the mouse IgM BG-1 antibody (BioLegend, San Diego, CA) coupled
414 to α-mouse IgM microbeads (Miltenyi Biotec, Bergisch Gladbach, Germany) (Table S1). Both
415 hESCs and hiPSCs were differentiated into the three germ layers. On d0 and d4 of each
416 differentiation, cells were harvested, dissociated, and filtered, as described above.
417 Approximately 5 x 10^6 cells of d0 and d4, respectively, were pooled in MACS buffer (0.5 %
418 (w/v) BSA and 2 mM EDTA in PBS, degassed) and stained with mouse IgM BG-1 antibody for
419 20 min at 4 °C followed by staining with 20 µl α-mouse IgM microbeads in MACS buffer in a
420 total volume of 100 µl for 15 min at 4 °C. Stained cells were washed twice with 1 ml PBS each
421 and resuspended in 2 ml MACS buffer. MACS was performed applying an autoMACS® Pro
422 Separator using autoMACS® columns (both Miltenyi Biotec) and the depletion program with a
423 flow rate of 0.25 ml/min. Cell surface expression of T1LN, SSEA-3, SSEA-4, and H-1 (SSEA-
424 5) was monitored pre-MACS in the d0-, d4-, and d0/d4-pooled population, as well as post-
425 MACS in the T1LN-positive and T1LN-negative population using flow cytometry. The data were
426 again processed using the FlowJo v7.6.4 software. Quantification of differentiation marker
427 expression on d4 was determined as described above. For quantification of cells positive for
428 T1LN, SSEA-3, SSEA-4, and H-1 (SSEA-5) viable cells were determined in an unstained
429 control of d0 for all pre- and post-MACS cell populations after ensuring that sorting did not
430 influence the set gate of viable cells. MFI values were again determined by the the FlowJo
431 v7.6.4 software and subtracted from the MFI of the respective isotype control. Due to a limited
432 number of cells, isotype controls were only carried out for the d0 and d4 population. Therefore,
433 the MFI of the pooled and the post-MACS populations were subtracted from the mean MFI of
434 the isotype controls of d0 and d4.

435 Isolation of RNA

436 Approximately 10^6 hESCs and hiPSCs were harvested on d0 and d4 of each differentiation,
437 respectively. Additionally, 10^6 cells of the d0/d4-pooled population and of the post-MACS
438 T1LN- positive and T1LN-negative population were collected for RNA isolation, cDNA
439 synthesis, and quantitative real-time PCR (qPCR) and stored at – 80 °C until further use. For
440 RNA isolation, cells were resuspended in TRIzol (250 µl, Life Technologies). RNA was
441 extracted by addition of 50 µl chloroform, short incubation, and centrifugation for 15 min at
442 11,000 x g. Isopropanol was added to the upper aqueous phase, followed by stirring,
443 incubation for 10 min, and centrifugation for 10 min at 11,000 x g. The pellet was washed in
444 250 µl ethanol (70 % (v/v)) and centrifuged again for 5 min at 11,000 x g. Residual ethanol was
445 removed and the extracted RNA pellet was resuspended in RNAse free water. Total RNA
446 concentration was determined from absorption at 260 nm using an UV spectrophotometer
447 (Implen, Munich, Germany). RNA was stored at – 80 °C until further use.

448 cDNA synthesis

449 cDNA was synthesized from 2.5 µg extracted RNA per sample in a total reaction volume of 50
450 µl. Residual genomic DNA was removed by digestion with RQ1 DNase (2.5 U, Promega) for
451 30 min at 37 °C. The reaction was stopped by adding RQ1 DNase stop solution and incubating
452 for 10 min at 70 °C. The cDNA was synthesized by using random hexamer primers (Thermo
453 Fisher Scientific). Primers were annealed for 10 min at 25 °C followed by cDNA synthesis using
454 Maxima H Minus Reverse Transcriptase (Thermo Fisher Scientific) and incubation for 30 min
455 at 50 °C. The reaction was stopped by heating for 5 min to 85 °C. All reaction steps were
456 performed in a Piko PCR cycler (Thermo Fisher Scientific). Synthesized cDNA was diluted in
457 water to 5 ng/µl and stored at – 20 °C.

458 Quantitative real-time PCR (RT-qPCR)

459 RT-qPCR was performed in a total reaction volume of 10 µl containing 15 ng cDNA, 2 pmol
460 forward/ reverse primer pairs (sequences listed in Table S2), and the BIO SyGreen Lo-ROX
461 mix (PCR Biosystems, London, UK) on an ImageQuantQ3 Real-time PCR System (Thermo
462 Fisher Scientific) in sealed 96-well optical reaction plates (Applied Biosystems). The specificity

463 of the designed primers was ensured by melting-curve analysis and sequencing of the
464 amplicon. The PCR was run for 40 two-step cycles (5 s at 95 °C, 30 s at 60 °C) after initial
465 denaturation for 2 min at 50 °C and 3 min at 95 °C. Amplicon purity was ensured by melting-
466 curve analysis in an additional cycle (15 s at 95 °C, 60 s at 60 °C, 15 s at 95 °C). Relative
467 expression of target genes was determined by normalization to house-keeping genes (listed
468 in Table S2). The ImageQuant software calculated cycle threshold (Ct) values automatically
469 and the relative expression of target genes were subsequently calculated by determination of
470 $2^{-\Delta\Delta Ct}$-values. Statistical analyses were performed using GraphPad Prism 5.01 software and *p*-
471 values of <0.05 upon unpaired Student's *t*-test were regarded as statistically significant.

472

473 ## Supplementary data

474 Supplementary data for this article are available at *Glycobiology* online.

475

476 ## Author contributions

477 C.R., S.B., J.B., A.O., M.D.A, and O.N. conducted the experiments, C.R. and F.F.R.B.
478 designed the experiments and performed data analysis and interpretation. F.F.R.B. conceived
479 and supervised this study. C.R. and F.F.R.B. wrote the manuscript, and all authors reviewed,
480 edited and agreed on its contents.

481

482 ## Acknowledgments

483 The authors would like to thank Prof. Dr. Gerardy-Schahn and Prof. Dr. Christoph Garbers,
484 Institute of Clinical Biochemistry, Hannover Medical School (MHH) for providing general
485 laboratory equipment.

486

487 ## Funding

488 This work was funded for F.F.R.B. by the Deutsche Forschungsgemeinschaft (DFG, German
489 Research Foundation) for Forschungsgruppe FOR2953 (Projektnummer: 409784463, project
490 P9; BU 2920/4-2) and for Forschungsgruppe FOR2509 (Projektnummer: 289991887, project
491 P3; BU 2920/2-2) and for the Cluster of Excellence REBIRTH (From Regenerative Biology to
492 Reconstructive Therapy, EXC 62).

493

494 ## Conflict of interest statement

495 The authors declare that they have no conflict of interest.

496

497 ## References

498 Barone, A., Benktander, J., Ångström, J., Aspegren, A., Björquist, P., Teneberg, S., and Breimer, M.E.
499 (2013). Structural complexity of non-acid glycosphingolipids in human embryonic stem cells grown
500 under feeder-free conditions. J Biol Chem *288*, 10035-10050. 10.1074/jbc.M112.436162.
501 Barone, A., Säljö, K., Benktander, J., Blomqvist, M., Månsson, J.E., Johansson, B.R., Mölne, J., Aspegren,
502 A., Björquist, P., Breimer, M.E., and Teneberg, S. (2014). Sialyl-lactotetra, a novel cell surface marker
503 of undifferentiated human pluripotent stem cells. J Biol Chem *289*, 18846-18859.
504 10.1074/jbc.M114.568832.
505 Carpenter, M.K., Rosler, E.S., Fisk, G.J., Brandenberger, R., Ares, X., Miura, T., Lucero, M., and Rao, M.S.
506 (2004). Properties of four human embryonic stem cell lines maintained in a feeder-free culture system.
507 Dev Dyn *229*, 243-258. 10.1002/dvdy.10431.
508 Chen, G., Gulbranson, D.R., Hou, Z., Bolin, J.M., Ruotti, V., Probasco, M.D., Smuga-Otto, K., Howden,
509 S.E., Diol, N.R., Propson, N.E., et al. (2011). Chemically defined conditions for human iPSC derivation
510 and culture. Nat Methods *8*, 424-429. 10.1038/nmeth.1593.
511 Choo, A.B., Tan, H.L., Ang, S.N., Fong, W.J., Chin, A., Lo, J., Zheng, L., Hentze, H., Philp, R.J., Oh, S.K., and
512 Yap, M. (2008). Selection against undifferentiated human embryonic stem cells by a cytotoxic antibody
513 recognizing podocalyxin-like protein-1. Stem Cells *26*, 1454-1463. 10.1634/stemcells.2007-0576.
514 Cumin, C., Huang, Y.L., Rossdam, C., Ruoff, F., Céspedes, S.P., Liang, C.Y., Lombardo, F.C., Coelho, R.,
515 Rimmer, N., Konantz, M., et al. (2022). Glycosphingolipids are mediators of cancer plasticity through
516 independent signaling pathways. Cell Rep *40*, 111181. 10.1016/j.celrep.2022.111181.
517 D'Angelo, G., Capasso, S., Sticco, L., and Russo, D. (2013). Glycosphingolipids: synthesis and functions.
518 Febs j *280*, 6338-6353. 10.1111/febs.12559.
519 Diekmann, U., Lenzen, S., and Naujok, O. (2015). A reliable and efficient protocol for human pluripotent
520 stem cell differentiation into the definitive endoderm based on dispersed single cells. Stem Cells Dev
521 *24*, 190-204. 10.1089/scd.2014.0143.
522 Domino, S.E., Zhang, L., Gillespie, P.J., Saunders, T.L., and Lowe, J.B. (2001). Deficiency of reproductive
523 tract alpha(1,2)fucosylated glycans and normal fertility in mice with targeted deletions of the FUT1 or

524 FUT2 alpha(1,2)fucosyltransferase locus. Mol Cell Biol *21*, 8336-8345. 10.1128/mcb.21.24.8336-
525 8345.2001.
526 Draper, J.S., Pigott, C., Thomson, J.A., and Andrews, P.W. (2002). Surface antigens of human embryonic
527 stem cells: changes upon differentiation in culture. J Anat *200*, 249-258. 10.1046/j.1469-
528 7580.2002.00030.x.
529 Fenderson, B.A., Andrews, P.W., Nudelman, E., Clausen, H., and Hakomori, S. (1987). Glycolipid core
530 structure switching from globo- to lacto- and ganglio-series during retinoic acid-induced differentiation
531 of TERA-2-derived human embryonal carcinoma cells. Dev Biol *122*, 21-34. 10.1016/0012-
532 1606(87)90328-9.
533 Fong, C.Y., Gauthaman, K., and Bongso, A. (2010). Teratomas from pluripotent stem cells: A clinical
534 hurdle. J Cell Biochem *111*, 769-781. 10.1002/jcb.22775.
535 Fujitani, N., Furukawa, J., Araki, K., Fujioka, T., Takegawa, Y., Piao, J., Nishioka, T., Tamura, T., Nikaido,
536 T., Ito, M., et al. (2013). Total cellular glycomics allows characterizing cells and streamlining the
537 discovery process for cellular biomarkers. Proc Natl Acad Sci U S A *110*, 2105-2110.
538 10.1073/pnas.1214233110.
539 Haase, A., Göhring, G., and Martin, U. (2017). Generation of non-transgenic iPS cells from human cord
540 blood CD34(+) cells under animal component-free conditions. Stem Cell Res *21*, 71-73.
541 10.1016/j.scr.2017.03.022.
542 Hasehira, K., Tateno, H., Onuma, Y., Ito, Y., Asashima, M., and Hirabayashi, J. (2012). Structural and
543 quantitative evidence for dynamic glycome shift on production of induced pluripotent stem cells. Mol
544 Cell Proteomics *11*, 1913-1923. 10.1074/mcp.M112.020586.
545 Ho, M.Y., Yu, A.L., and Yu, J. (2017). Glycosphingolipid dynamics in human embryonic stem cell and
546 cancer: their characterization and biomedical implications. Glycoconj J *34*, 765-777. 10.1007/s10719-
547 016-9715-x.
548 Jirmo, A.C., Rossdam, C., Grychtol, R., Happle, C., Gerardy-Schahn, R., Buettner, F.F.R., and Hansen, G.
549 (2020). Differential expression patterns of glycosphingolipids and C-type lectin receptors on immune
550 cells in absence of functional regulatory T cells. Immun Inflamm Dis *8*, 512-522. 10.1002/iid3.334.
551 Kannagi, R., Cochran, N.A., Ishigami, F., Hakomori, S., Andrews, P.W., Knowles, B.B., and Solter, D.
552 (1983). Stage-specific embryonic antigens (SSEA-3 and -4) are epitopes of a unique globo-series
553 ganglioside isolated from human teratocarcinoma cells. Embo j *2*, 2355-2361. 10.1002/j.1460-
554 2075.1983.tb01746.x.
555 Kempf, H., Andree, B., and Zweigerdt, R. (2016a). Large-scale production of human pluripotent stem
556 cell derived cardiomyocytes. Adv Drug Deliv Rev *96*, 18-30. 10.1016/j.addr.2015.11.016.
557 Kempf, H., Olmer, R., Haase, A., Franke, A., Bolesani, E., Schwanke, K., Robles-Diaz, D., Coffee, M.,
558 Göhring, G., Dräger, G., et al. (2016b). Bulk cell density and Wnt/TGFbeta signalling regulate
559 mesendodermal patterning of human pluripotent stem cells. Nat Commun *7*, 13602.
560 10.1038/ncomms13602.
561 Konze, S.A., Cajic, S., Oberbeck, A., Hennig, R., Pich, A., Rapp, E., and Buettner, F.F.R. (2017).
562 Quantitative Assessment of Sialo-Glycoproteins and N-Glycans during Cardiomyogenic Differentiation
563 of Human Induced Pluripotent Stem Cells. Chembiochem *18*, 1317-1331. 10.1002/cbic.201700100.
564 Liang, Y.J., Kuo, H.H., Lin, C.H., Chen, Y.Y., Yang, B.C., Cheng, Y.Y., Yu, A.L., Khoo, K.H., and Yu, J. (2010).
565 Switching of the core structures of glycosphingolipids from globo- and lacto- to ganglio-series upon
566 human embryonic stem cell differentiation. Proc Natl Acad Sci U S A *107*, 22564-22569.
567 10.1073/pnas.1007290108.
568 Liang, Y.J., Yang, B.C., Chen, J.M., Lin, Y.H., Huang, C.L., Cheng, Y.Y., Hsu, C.Y., Khoo, K.H., Shen, C.N.,
569 and Yu, J. (2011). Changes in glycosphingolipid composition during differentiation of human embryonic
570 stem cells to ectodermal or endodermal lineages. Stem Cells *29*, 1995-2004. 10.1002/stem.750.
571 Lin, R.J., Kuo, M.W., Yang, B.C., Tsai, H.H., Chen, K., Huang, J.R., Lee, Y.S., Yu, A.L., and Yu, J. (2020).
572 B3GALT5 knockout alters gycosphingolipid profile and facilitates transition to human naïve
573 pluripotency. Proc Natl Acad Sci U S A *117*, 27435-27444. 10.1073/pnas.2003155117.
574 Natunen, S., Satomaa, T., Pitkänen, V., Salo, H., Mikkola, M., Natunen, J., Otonkoski, T., and Valmu, L.
575 (2011). The binding specificity of the marker antibodies Tra-1-60 and Tra-1-81 reveals a novel

576 pluripotency-associated type 1 lactosamine epitope. Glycobiology *21*, 1125-1130.
577 10.1093/glycob/cwq209.
578 Naujok, O., Kaldrack, J., Taivankhuu, T., Jörns, A., and Lenzen, S. (2010). Selective removal of
579 undifferentiated embryonic stem cells from differentiation cultures through HSV1 thymidine kinase
580 and ganciclovir treatment. Stem Cell Rev Rep *6*, 450-461. 10.1007/s12015-010-9148-z.
581 Ojima, T., Shibata, E., Saito, S., Toyoda, M., Nakajima, H., Yamazaki-Inoue, M., Miyagawa, Y., Kiyokawa,
582 N., Fujimoto, J.I., Sato, T., and Umezawa, A. (2015). Glycolipid dynamics in generation and
583 differentiation of induced pluripotent stem cells. Sci Rep *5*, 14988. 10.1038/srep14988.
584 Okano, H., and Yamanaka, S. (2014). iPS cell technologies: significance and applications to CNS
585 regeneration and disease. Mol Brain *7*, 22. 10.1186/1756-6606-7-22.
586 Pera, M.F., and Trounson, A.O. (2004). Human embryonic stem cells: prospects for development.
587 Development *131*, 5515-5525. 10.1242/dev.01451.
588 Rossdam, C., Konze, S.A., Oberbeck, A., Rapp, E., Gerardy-Schahn, R., von Itzstein, M., and Buettner,
589 F.F.R. (2019). Approach for Profiling of Glycosphingolipid Glycosylation by Multiplexed Capillary Gel
590 Electrophoresis Coupled to Laser-Induced Fluorescence Detection To Identify Cell-Surface Markers of
591 Human Pluripotent Stem Cells and Derived Cardiomyocytes. Anal Chem *91*, 6413-6418.
592 10.1021/acs.analchem.9b01114.
593 Russo, D., Capolupo, L., Loomba, J.S., Sticco, L., and D'Angelo, G. (2018). Glycosphingolipid metabolism
594 in cell fate specification. J Cell Sci *131*. 10.1242/jcs.219204.
595 Säljö, K., Barone, A., Vizlin-Hodzic, D., Johansson, B.R., Breimer, M.E., Funa, K., and Teneberg, S. (2017).
596 Comparison of the glycosphingolipids of human-induced pluripotent stem cells and human embryonic
597 stem cells. Glycobiology *27*, 291-305. 10.1093/glycob/cww125.
598 Shi, Y., Kirwan, P., and Livesey, F.J. (2012). Directed differentiation of human pluripotent stem cells to
599 cerebral cortex neurons and neural networks. Nat Protoc *7*, 1836-1846. 10.1038/nprot.2012.116.
600 Starzonek, S., Maar, H., Labitzky, V., Wicklein, D., Rossdam, C., Buettner, F.F.R., Wolters-Eisfeld, G.,
601 Guengoer, C., Wagener, C., Schumacher, U., and Lange, T. (2020). Systematic analysis of the human
602 tumor cell binding to human vs. murine E- and P-selectin under static vs. dynamic conditions.
603 Glycobiology *30*, 695-709. 10.1093/glycob/cwaa019.
604 Tan, H.L., Fong, W.J., Lee, E.H., Yap, M., and Choo, A. (2009). mAb 84, a cytotoxic antibody that kills
605 undifferentiated human embryonic stem cells via oncosis. Stem Cells *27*, 1792-1801.
606 10.1002/stem.109.
607 Tang, C., Lee, A.S., Volkmer, J.P., Sahoo, D., Nag, D., Mosley, A.R., Inlay, M.A., Ardehali, R., Chavez, S.L.,
608 Pera, R.R., et al. (2011). An antibody against SSEA-5 glycan on human pluripotent stem cells enables
609 removal of teratoma-forming cells. Nat Biotechnol *29*, 829-834. 10.1038/nbt.1947.
610 Tateno, H., Toyota, M., Saito, S., Onuma, Y., Ito, Y., Hiemori, K., Fukumura, M., Matsushima, A.,
611 Nakanishi, M., Ohnuma, K., et al. (2011). Glycome diagnosis of human induced pluripotent stem cells
612 using lectin microarray. J Biol Chem *286*, 20345-20353. 10.1074/jbc.M111.231274.
613 Thiesler, C.T., Cajic, S., Hoffmann, D., Thiel, C., van Diepen, L., Hennig, R., Sgodda, M., Weiβmann, R.,
614 Reichl, U., Steinemann, D., et al. (2016). Glycomic Characterization of Induced Pluripotent Stem Cells
615 Derived from a Patient Suffering from Phosphomannomutase 2 Congenital Disorder of Glycosylation
616 (PMM2-CDG). Mol Cell Proteomics *15*, 1435-1452. 10.1074/mcp.M115.054122.
617 Wright, A.J., and Andrews, P.W. (2009). Surface marker antigens in the characterization of human
618 embryonic stem cells. Stem Cell Res *3*, 3-11. 10.1016/j.scr.2009.04.001.
619 Zhou, D., Henion, T.R., Jungalwala, F.B., Berger, E.G., and Hennet, T. (2000). The beta 1,3-
620 galactosyltransferase beta 3GalT-V is a stage-specific embryonic antigen-3 (SSEA-3) synthase. J Biol
621 Chem *275*, 22631-22634. 10.1074/jbc.C000263200.

622

623

624

625 # Figures

626 **Figure 1**

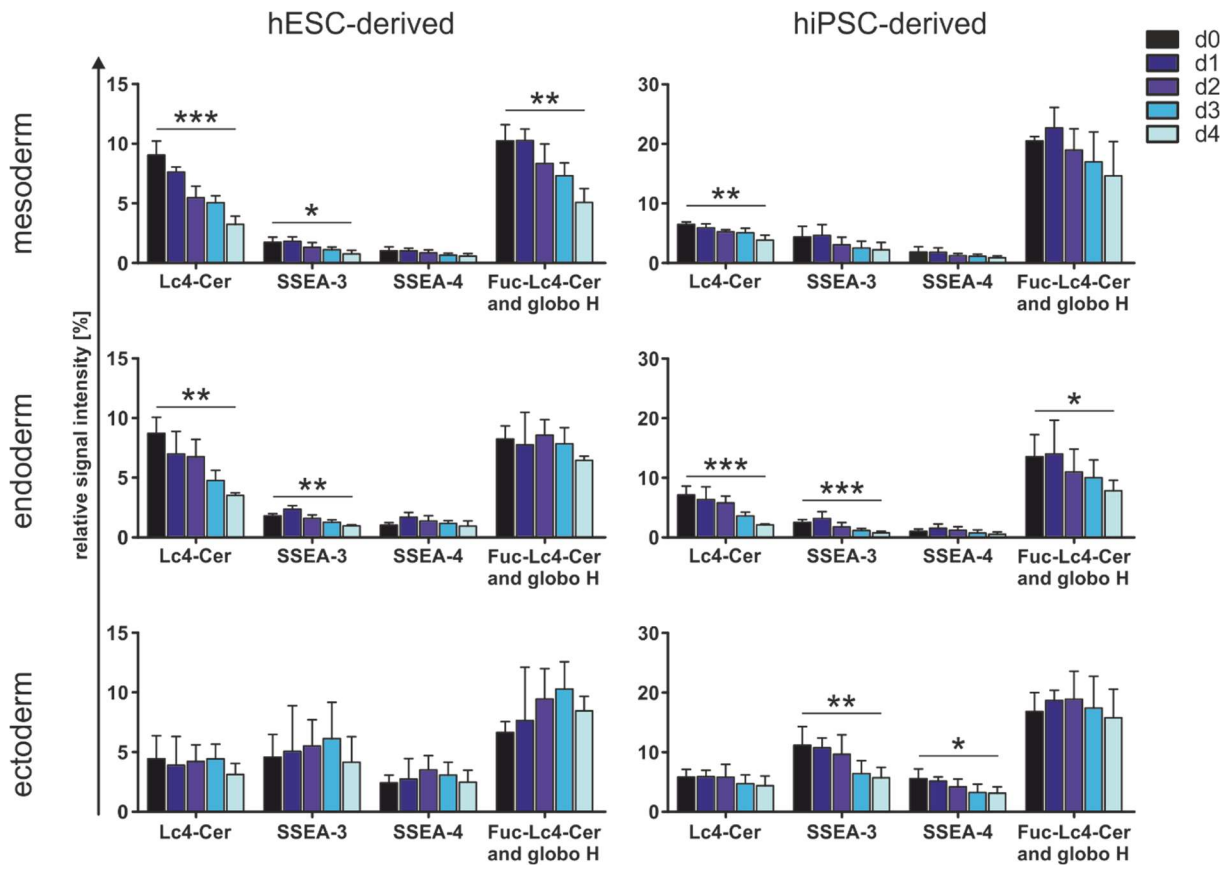

627

628 **Figure 1. GSL analysis**

629 xCGE-LIF analysis of APTS-labelled glycans derived from GSLs of hiPSCs (left panel) and
630 hESCs (right panel), and their differentiation derivatives of mesoderm (top), endoderm
631 (middle), and ectoderm (bottom) through days 0 - 4 of differentiation (d0-d4, black to light blue),
632 respectively. Relative signal intensities are displayed for Lc4-Cer, SSEA-3, SSEA-4, and
633 fucosyl Lc4-Cer / globo H. Bar diagrams represent mean + S.D. (*n*=3-5). An unpaired Student's
634 *t*-test was performed between the peaks of d0 and d4 of differentiation for each cell line and
635 each differentiation approach. Statistically significant differences are highlighted (* $p<0.05$;
636 ** $p<0.01$; *** $p<0.001$).

637

638

Figure 2

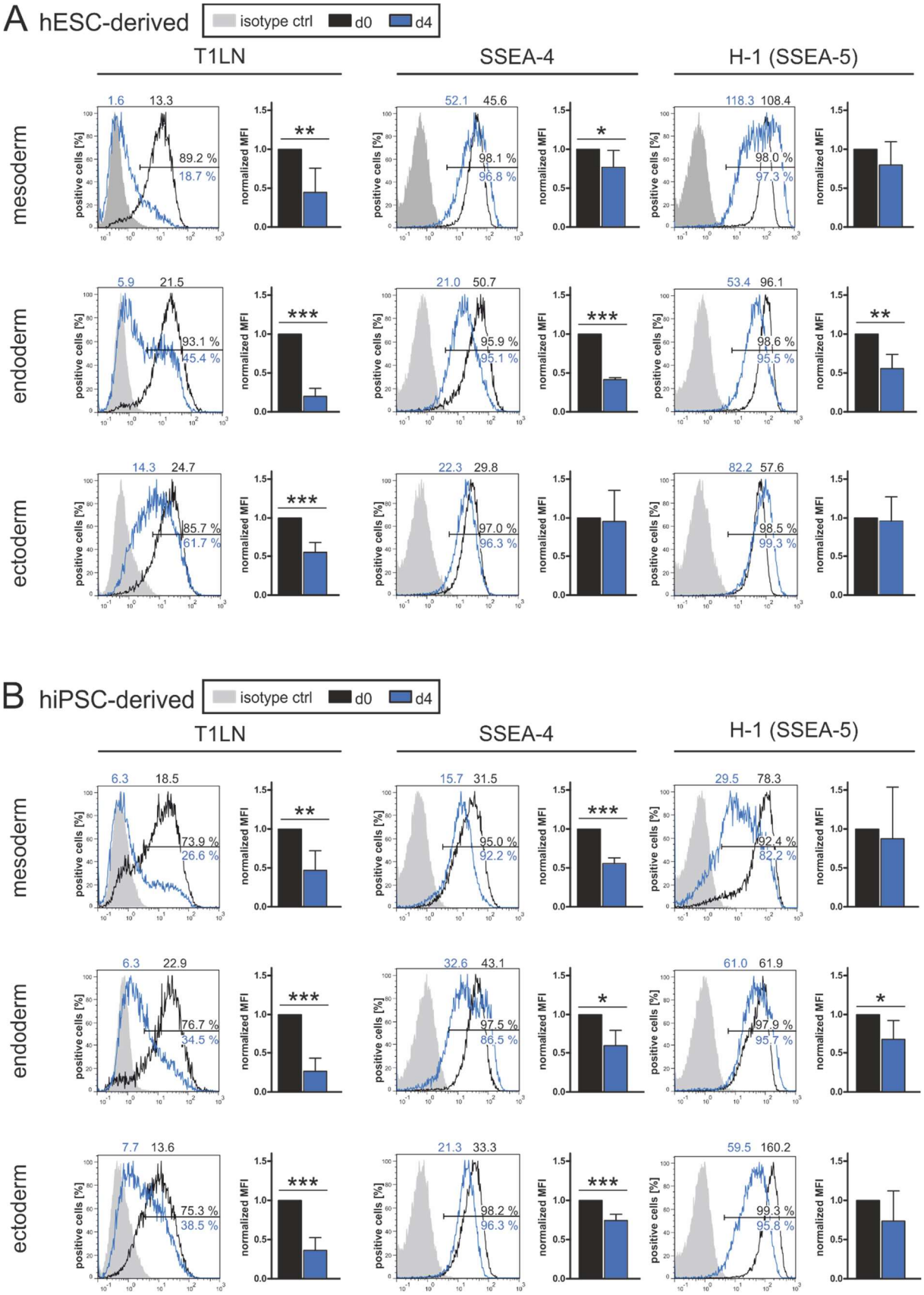
A hESC-derived
isotype ctrl
d0
d4
T1LN
SSEA-4
H-1 (SSEA-5)
mesoderm
endoderm
ectoderm
positive cells [%]
normalized MFI
1.6 13.3
89.2 %
18.7 %
52.1 45.6
98.1 %
96.8 %
118.3 108.4
98.0 %
97.3 %
5.9 21.5
93.1 %
45.4 %
21.0 50.7
95.9 %
95.1 %
53.4 96.1
98.6 %
95.5 %
14.3 24.7
85.7 %
61.7 %
22.3 29.8
97.0 %
96.3 %
82.2 57.6
98.5 %
99.3 %
B hiPSC-derived
isotype ctrl
d0
d4
T1LN
SSEA-4
H-1 (SSEA-5)
mesoderm
endoderm
ectoderm
positive cells [%]
normalized MFI
6.3 18.5
73.9 %
26.6 %
15.7 31.5
95.0 %
92.2 %
29.5 78.3
92.4 %
82.2 %
6.3 22.9
76.7 %
34.5 %
32.6 43.1
97.5 %
86.5 %
61.0 61.9
97.9 %
95.7 %
7.7 13.6
75.3 %
38.5 %
21.3 33.3
98.2 %
96.3 %
59.5 160.2
99.3 %
95.8 %

642 **Figure 2. Cell surface expression of T1LN, SSEA-4, and SSEA-5**

643 (A-B) Flow cytometry analysis of hESCs (A) and hiPSCs (B) on d0 and d4 of differentiation for
644 each differentiation approach (top: mesoderm; middle: endoderm; bottom: ectoderm) for T1LN
645 (left panel), SSEA-4 (middle panel), and SSEA-5 (right panel). Representative overlay
646 histograms show fluorescence signal of viable cells on d0 (black) and d4 (blue). Cells were
647 defined positive if the fluorescence signal was above that of 99 % of the cells stained with the
648 respective isotype control (grey). Only isotype controls for d0 are displayed, but for calculation
649 of positive cells on d4, isotype controls of d4 were considered. Number of positive cells are
650 shown below (blue) and above (black) the line representing the gate. Mean fluorescence
651 intensity is shown above histograms (d0, black and d4, blue). Bar diagrams show mean
652 fluorescence intensities (MFI) + S.D. (n=3-6) normalized to d0. An unpaired Student's t-test
653 was performed for each target between d0 and d4 of differentiation and statistically significant
654 differences are highlighted (* p<0.05; ** p<0.01; *** p<0.001).

655

656

657

658

659

660

661

662

663

664

665

666

667

668

669 **Figure 3 A and B**

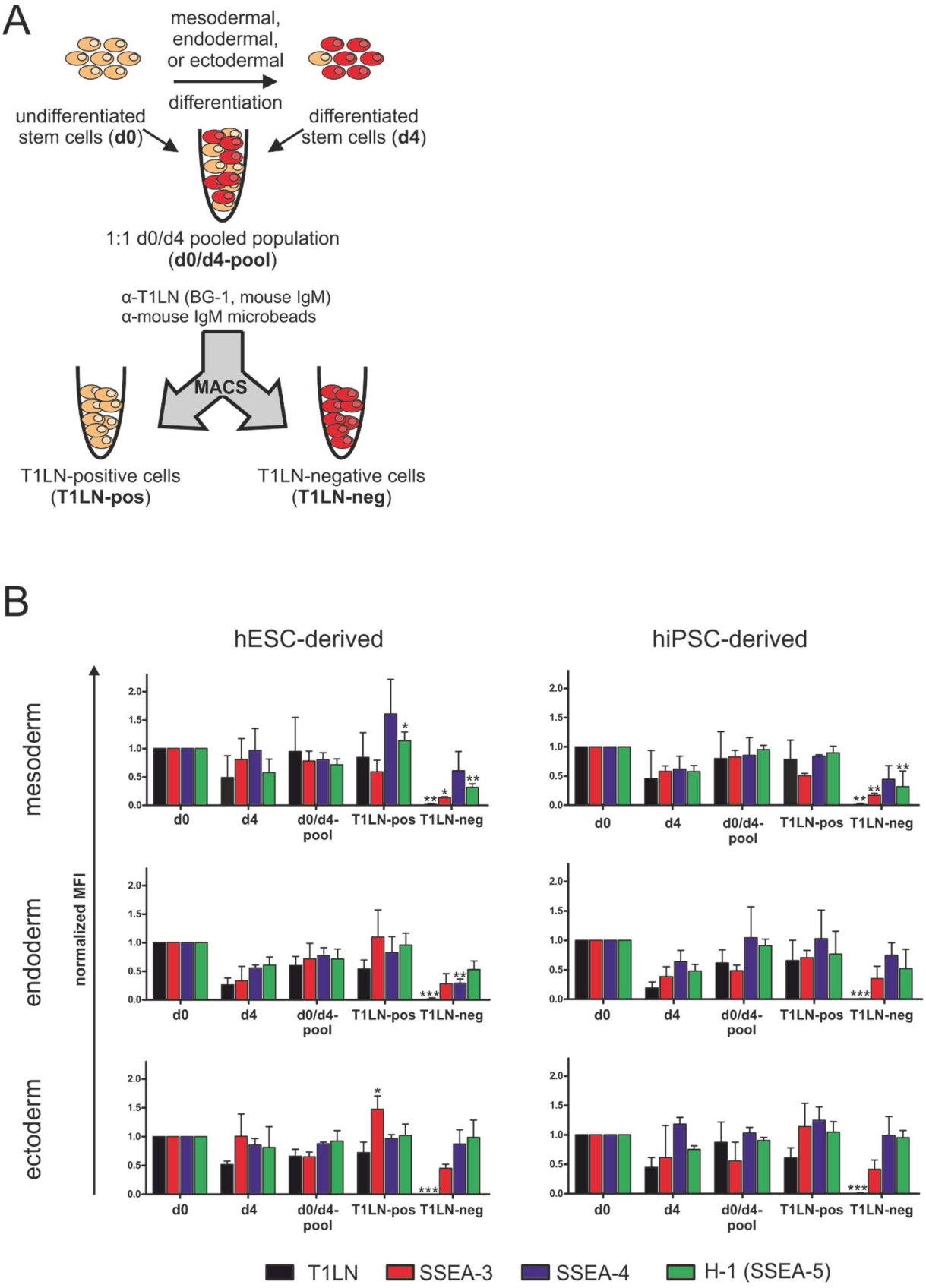

670

671

672 **Figure 3 C**

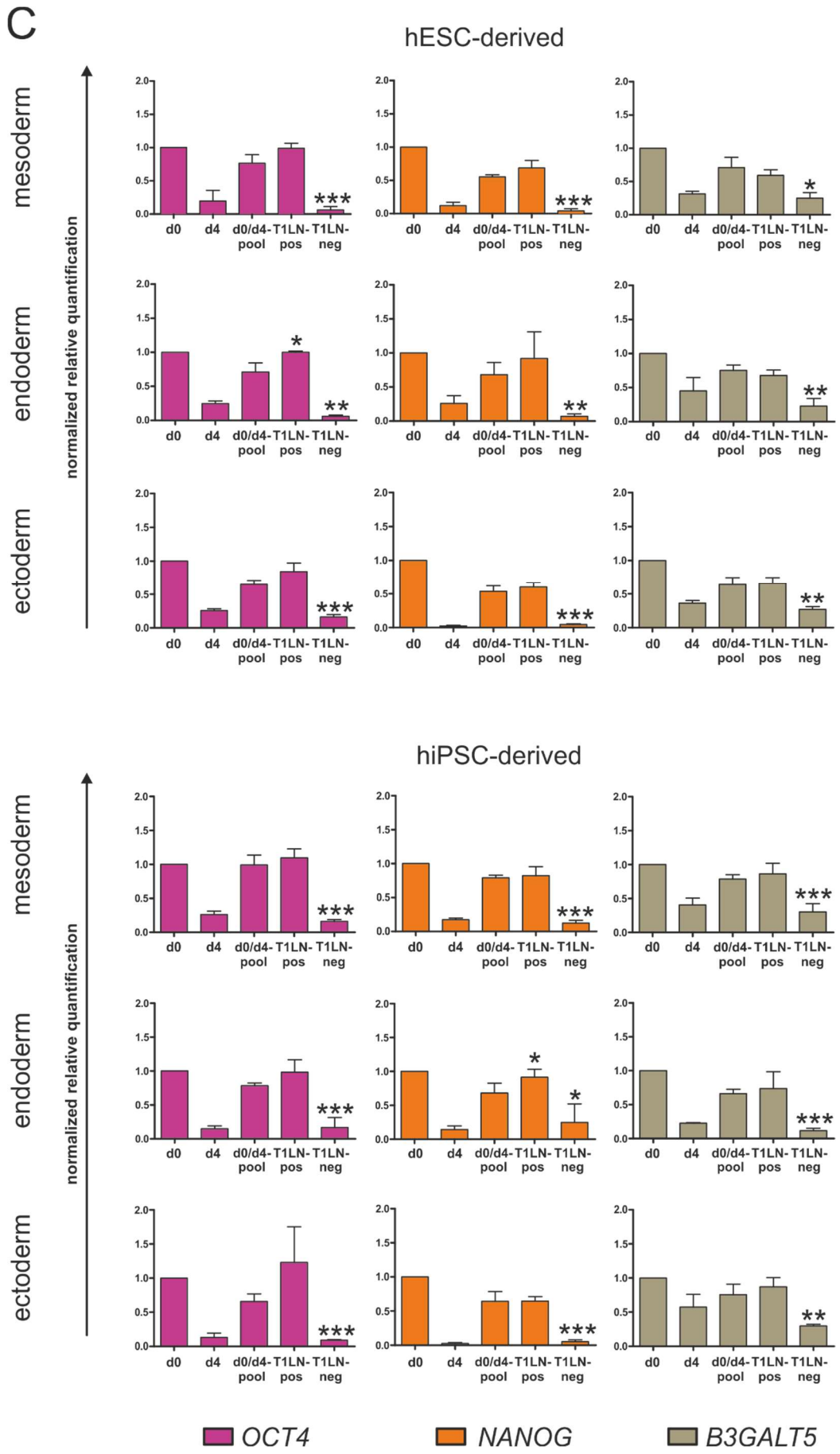

673

674 **Figure 3. Cell sorting and analysis of T1LN, SSEA-3, SSEA-4, and SSEA-5**

675 (A) Schematic illustration of MACS assay using a 1:1 pool of undifferentiated stem cells (d0,
676 shown in orange) and differentiated stem cells (d4, shown in red) (d0/d4-pool). Cell sorting
677 using the mouse IgM antibody BG-1 directed against T1LN and α-mouse IgM microbeads
678 generated a pool of T1LN-positive cells (T1LN-pos) and T1LN-negative cells (T1LN-neg).
679 (B) Cell surface expression of T1LN, SSEA-3, SSEA-4, and SSEA-5 in hPSCs and
680 differentiated derivatives pre- and post-MACS using the α-T1LN antibody. Bar diagrams show
681 mean fluorescence intensities (MFI, normalized to d0) + S.D. (n=3-7) of T1LN (black), SSEA-
682 3 (red), SSEA-4 (blue), and SSEA-5 (green).
683 (C) Relative expression of *OCT4*, *NANOG,* and β-1-3-galactosyltransferase *B3GALT5* in
684 hPSCs and differentiated derivatives pre- and post-MACS analyzed by qPCR. Error bars
685 represent mean + S.D. (n=3-4). For both B and C, expression was analyzed in hESCs (left
686 panel) and hiPSCs (right panel) and their differentiated derivatives (top: mesoderm; middle:
687 endoderm; bottom: ectoderm) pre-MACS in d0, d4 and d0/d4-pooled cells, as well as post-
688 MACS in the T1LN-positive and T1LN-negative population. An unpaired Student's *t*-test was
689 performed for each target between d0/d4-pool and T1LN-pos or T1LN-neg, respectively, and
690 statistically significant differences are highlighted (* p<0.05; ** p<0.01; *** p<0.001).
691

692

693 **Figure 4**

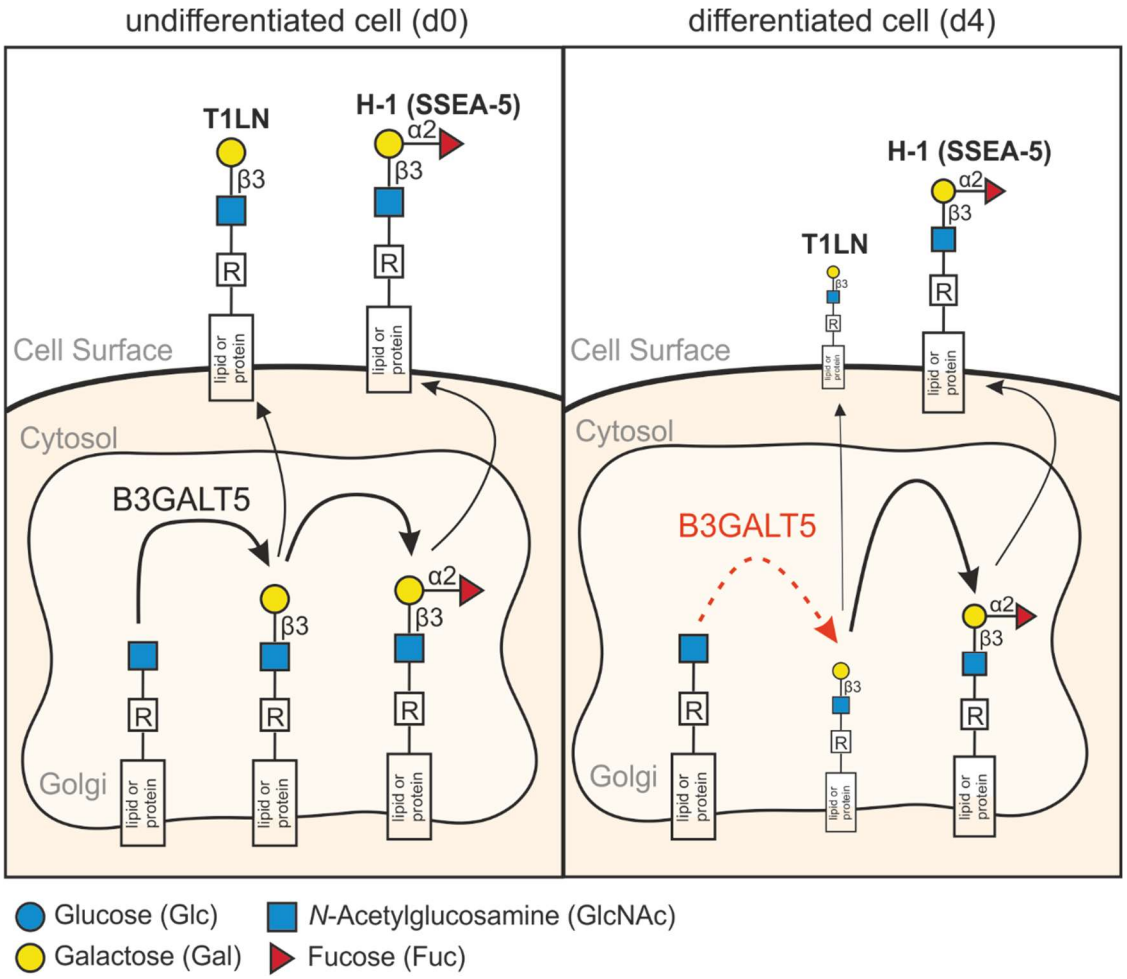

694

695 **Figure 4. Model for T1LN expression during differentiation of hPSCs**

696 In hPSCs (d0, left) B3GALT5 is highly expressed leading to continuous synthesis of protein
697 and lipid-bound glycans decorated with T1LN structures that can be further elongated by
698 fucosylation into H-1 epitopes which are target structures for the SSEA-5 antibody. During
699 differentiation (e.g. on d4, right) expression of B3GALT4 drops and synthesis of glycans with
700 T1LN epitopes is reduced while these glycans are still continuously fucosylated into H-1
701 structures. Therefore, levels of glycans with T1LN structures decrease more rapidly that H-1
702 glycans.

703

704 **Supplementary information**

705

706 Targeting the glycan epitope type I *N*-acetyllactosamine 707 enables immunodepletion of human pluripotent stem cells 708 from early differentiated cells

709

710 Charlotte Rossdam,[1] Smilla Brand,[1] Julia Beimdiek,[1] Astrid Oberbeck,[1] Marco Darius Albers,[1]
711 Ortwin Naujok,[1] and Falk F. R. Buettner[1,*]

712

713 [1]Institute of Clinical Biochemistry, Hannover Medical School, 30625 Hannover, Germany

714 *Correspondence: buettner.falk@mh-hannover.de (F.F.R.B.)

715 **Table S1. Antibodies used for flow cytometry and magnetic activated cell sorting.**

Primary antibodies and conjugated antibodies					
Target	**Host species (isotype)**	**Supplier**	**Order #**	**Dilution**	**Conjugated fluorochrome**
CXCR4 (CD184)	recombinant human IgG1	Miltenyi Biotec	130-117-504	1:50	PE
EpCAM (CD326)	recombinant human IgG1	Miltenyi Biotec	130-111-116	1:50	PE
IgG1 control	mouse IgG1, κ	Miltenyi Biotec	130-113-196	1:50	APC
IgG1 control	recombinant human IgG1	Miltenyi Biotec	130-120-709	1:50	APC
IgG1 control	recombinant human IgG1	Miltenyi Biotec	130-104-613	1:50	PE
IgG_{2b} control	mouse IgG_{2b}	BD Biosciences	565381	1:100	APC
IgM control	mouse IgM, κ	Miltenyi Biotec	130-120-070	1:50	PE
BG1	mouse IgM, κ	Biolegend	932102	1:100	/
NCAM (CD56)	mouse IgG_{2b}	BD Biosciences	341027	1:100	APC
Pax-6[1]	rabbit IgG	BioLegend	901301	1:50	/
Pax-6	rabbit IgG	Proteintech	12323-1-AP	1:100	/
SSEA-3	Rat IgM	Thermo Fisher Scientific	MA1-020-D650	1:100	DyLight 650
SSEA-4	recombinant human IgG1	Miltenyi Biotec	130-098-347	1:10	APC
SSEA-5	mouse IgG1, κ	Miltenyi Biotec	130-106-661	1:10	APC
Secondary antibodies and conjugated microbeads					
Target	**Host species (isotype)**	**Supplier**	**Order #**	**Dilution**	**Fluorochrome / microbeads**
mouse IgM	rat	BD Biosciences	553409	1:50	PE

mouse IgM	rat	Miltenyi Biotec	130-047-302	1:5	microbeads
rabbit IgG	goat	Molecular Probes	A21245	1:1200	Alexa 647

716 [1]The anti-Pax-6 antibody (901301) from BioLegend was unavailable for a long period due to difficulties
717 in shipping. Therefore, for experiments shown in Fig. 2, Fig 3, as well as SFig. 2, and SFig 4 the anti-
718 Pax-6 antibody (12323-1-AP) from Proteintech was used.

719 **Table S2. Oligonucleotides used as primers for qPCR.**

Target name	Primer name	Primer sequence (5' to 3')
Reference gene		
PGK1	PGK1_fw	AAGTCGGTAGTCCTTATGAGC
	PGK1_rev	CACATGAAAGCGGAGGTTCT
PPIA	PPIA_fw	GCCAAGACTGAGTGGTTGGAT
	PPIA_rev	GGCCTCCACAATATTCATGCC
RPLP0	RPLP0_fw	TGGTCATCCAGCAGGTGTTCGA
	RPLP0_rev	ACAGACACTGGCAACATTGCGG
Targets		
B3GALT5	B3GALT5_fw	CCAAGAGCGTCCCATACATTA
	B3GALT5_rev	CTGAAGAGGCATACGGAGAAG
NANOG	NANOG_fw	TACCTCAGCCTCCAGCAGAT
	NANOG_rev	TGCGTCACACCATTGCTATT
OCT4	OCT4_fw	AGAAGGAGAAGTUGGAGCAA
	OCT4_rev	CTTCCCAAATAGAACCCCCA

720

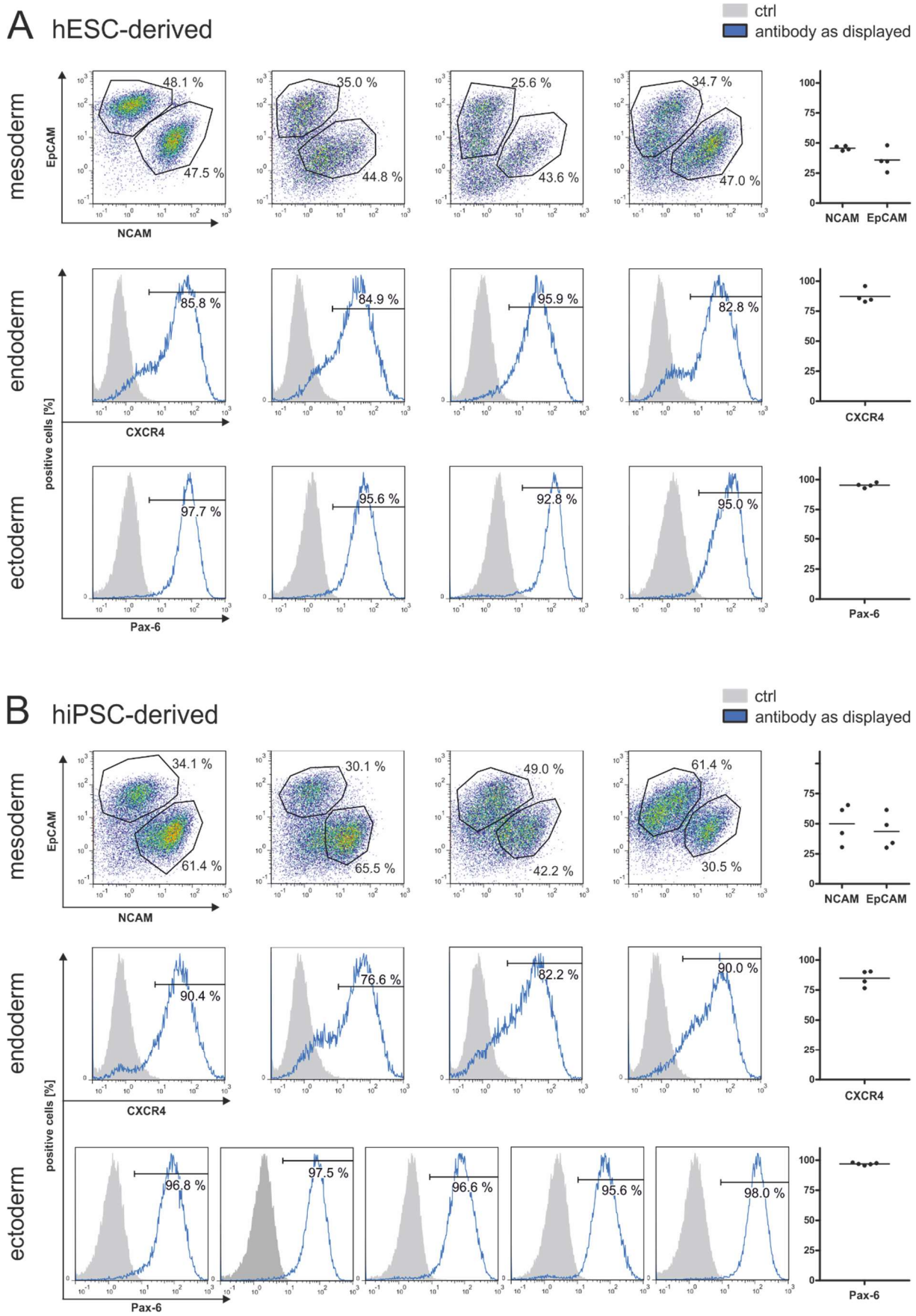
A hESC-derived
ctrl
antibody as displayed
mesoderm
EpCAM
NCAM
48.1 %
47.5 %
35.0 %
44.8 %
25.6 %
43.6 %
34.7 %
47.0 %
NCAM EpCAM
endoderm
positive cells [%]
CXCR4
85.8 %
84.9 %
95.9 %
82.8 %
ectoderm
Pax-6
97.7 %
95.6 %
92.8 %
95.0 %
B hiPSC-derived
34.1 %
61.4 %
30.1 %
65.5 %
49.0 %
42.2 %
61.4 %
30.5 %
90.4 %
76.6 %
82.2 %
90.0 %
96.8 %
97.5 %
96.6 %
95.6 %
98.0 %

721

722

723 **Supplemental Figure 1. Quality control of differentiation approaches of**
724 **replicates shown in Figure 1**

725 (A-B) Differentiation of hESCs (A) and hiPSCs (B) into mesoderm (top panel),
726 endoderm (middle panel), and ectoderm (bottom panel) was confirmed by cell surface
727 staining of corresponding differentiation markers and quantified via flow cytometry. For
728 mesoderm, dot plots are displayed showing balanced NCAM and EpCAM expression
729 in viable cells on d4 of differentiation. For endoderm and ectoderm, overlay histograms
730 show fluorescence signal of viable cells on d4 of differentiation (blue) for CXCR4 and
731 Pax-6, respectively. Cells were defined positive if the fluorescence signal was above
732 that of 99 % of the cells stained with the respective control (ctrl, grey). Scatter plots
733 display all analyzed replicates shown in Figure 1.

734

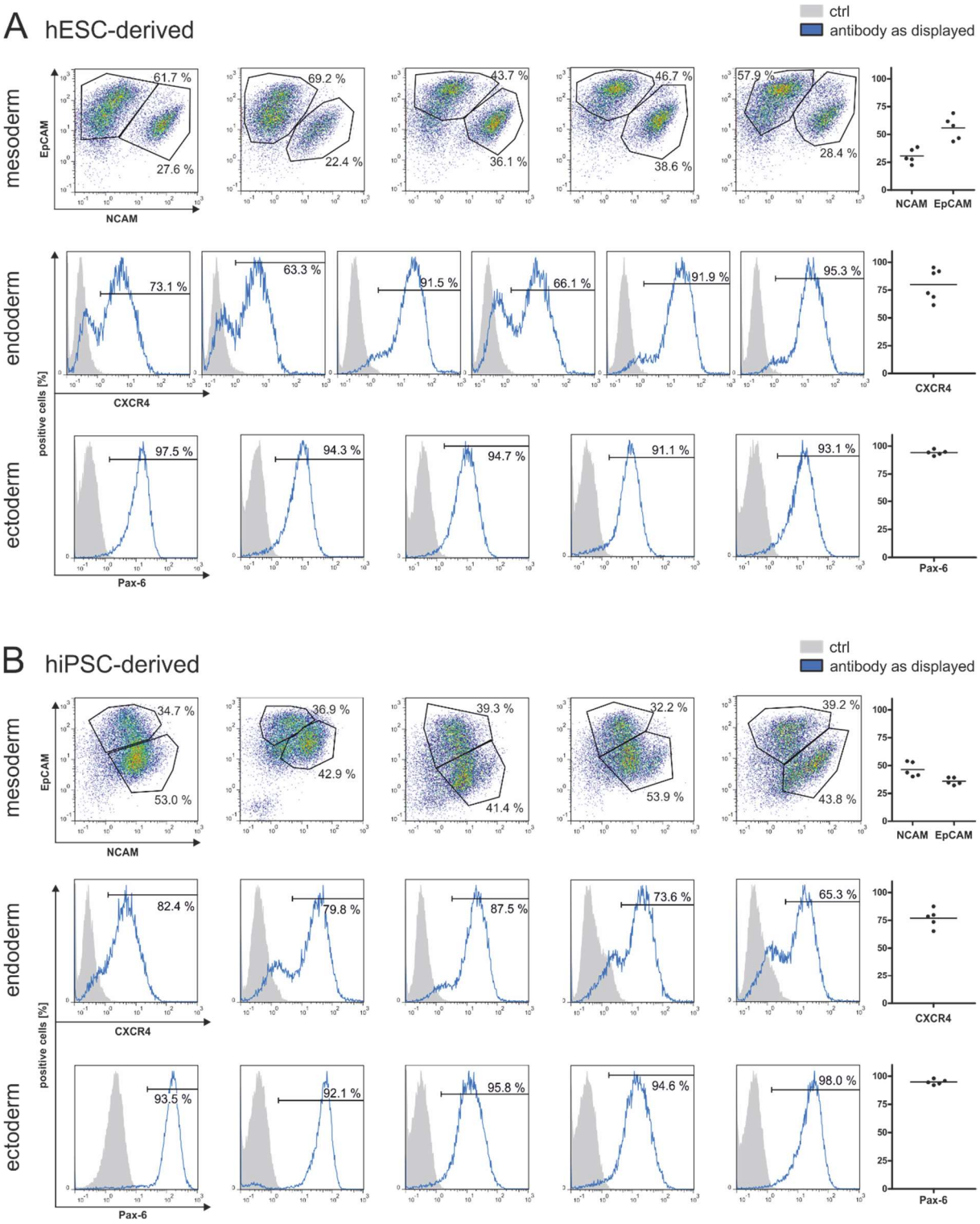
A hESC-derived
ctrl
antibody as displayed
mesoderm
endoderm
ectoderm
EpCAM
NCAM
CXCR4
Pax-6
positive cells [%]
61.7 %
27.6 %
69.2 %
22.4 %
43.7 %
36.1 %
46.7 %
38.6 %
57.9 %
28.4 %
73.1 %
63.3 %
91.5 %
66.1 %
91.9 %
95.3 %
97.5 %
94.3 %
94.7 %
91.1 %
93.1 %
B hiPSC-derived
ctrl
antibody as displayed
34.7 %
53.0 %
36.9 %
42.9 %
39.3 %
41.4 %
32.2 %
53.9 %
39.2 %
43.8 %
82.4 %
79.8 %
87.5 %
73.6 %
65.3 %
93.5 %
92.1 %
95.8 %
94.6 %
98.0 %

735

736 **Supplemental Figure 2. Quality control of differentiation approaches of**
737 **replicates shown in Figure 2**

738 (A-B) Differentiation of hESCs (A) and hiPSCs (B) into mesoderm (top panel),
739 endoderm (middle panel), and ectoderm (bottom panel) was confirmed by cell surface
740 staining of corresponding differentiation markers and quantified via flow cytometry. For
741 mesoderm, dot plots are displayed showing balanced NCAM and EpCAM expression
742 in viable cells on d4 of differentiation. For endoderm and ectoderm, overlay histograms
743 show fluorescence signal of viable cells on d4 of differentiation (blue) for CXCR4 and
744 Pax-6, respectively. Cells were defined positive if the fluorescence signal was above
745 that of 99 % of the cells stained with the respective control (ctrl, grey). Scatter plots
746 display all analyzed replicates shown in Figure 2.

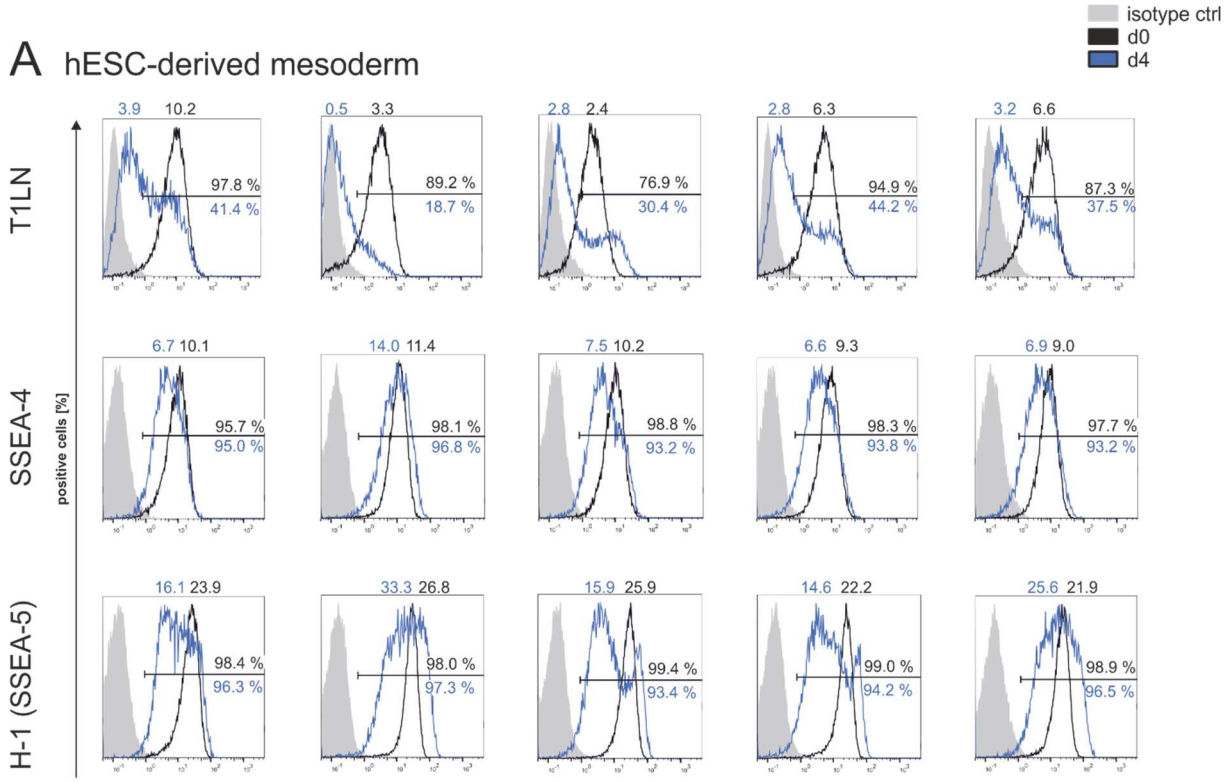
A hESC-derived mesoderm
isotype ctrl
d0
d4
T1LN
SSEA-4
H-1 (SSEA-5)
positive cells [%]
3.9 10.2
97.8 %
41.4 %
0.5 3.3
89.2 %
18.7 %
2.8 2.4
76.9 %
30.4 %
2.8 6.3
94.9 %
44.2 %
3.2 6.6
87.3 %
37.5 %
6.7 10.1
95.7 %
95.0 %
14.0 11.4
98.1 %
96.8 %
7.5 10.2
98.8 %
93.2 %
6.6 9.3
98.3 %
93.8 %
6.9 9.0
97.7 %
93.2 %
16.1 23.9
98.4 %
96.3 %
33.3 26.8
98.0 %
97.3 %
15.9 25.9
99.4 %
93.4 %
14.6 22.2
99.0 %
94.2 %
25.6 21.9
98.9 %
96.5 %

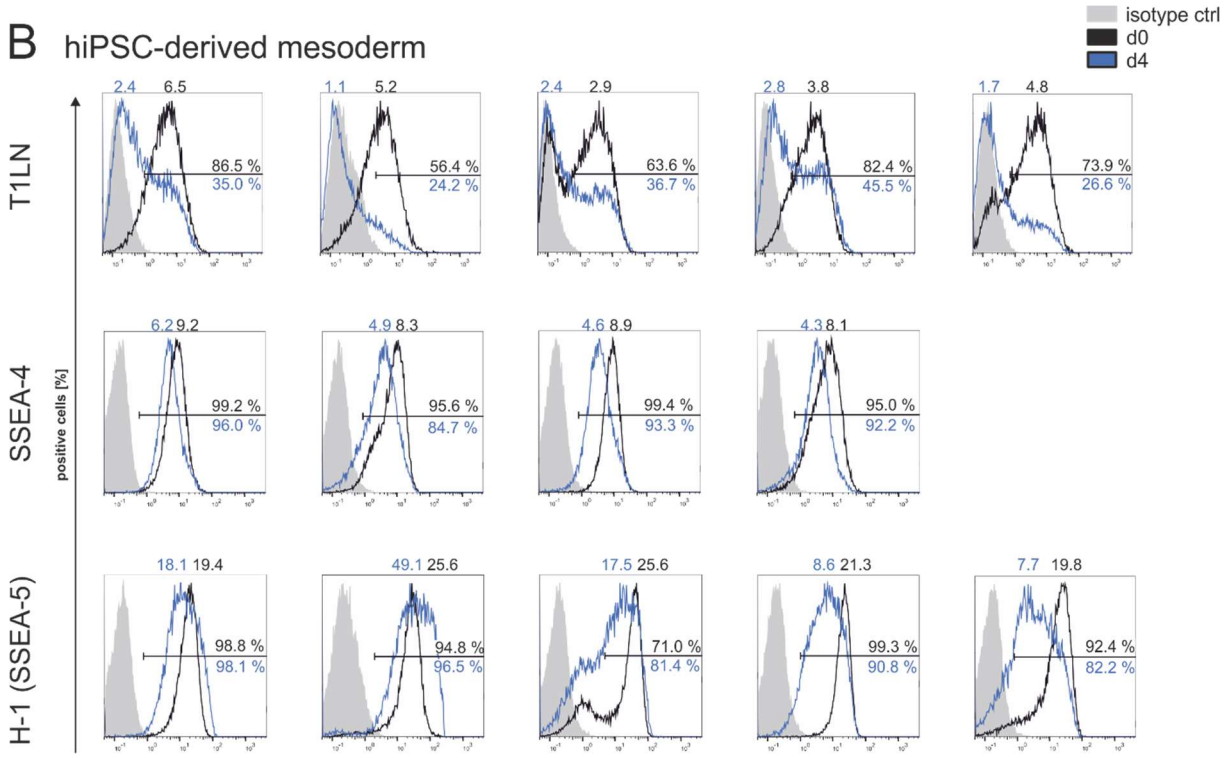
B hiPSC-derived mesoderm
isotype ctrl
d0
d4
T1LN
SSEA-4
H-1 (SSEA-5)
positive cells [%]
2.4 6.5
86.5 %
35.0 %
1.1 5.2
56.4 %
24.2 %
2.4 2.9
63.6 %
36.7 %
2.8 3.8
82.4 %
45.5 %
1.7 4.8
73.9 %
26.6 %
6.2 9.2
99.2 %
96.0 %
4.9 8.3
95.6 %
84.7 %
4.6 8.9
99.4 %
93.3 %
4.3 8.1
95.0 %
92.2 %
18.1 19.4
98.8 %
98.1 %
49.1 25.6
94.8 %
96.5 %
17.5 25.6
71.0 %
81.4 %
8.6 21.3
99.3 %
90.8 %
7.7 19.8
92.4 %
82.2 %

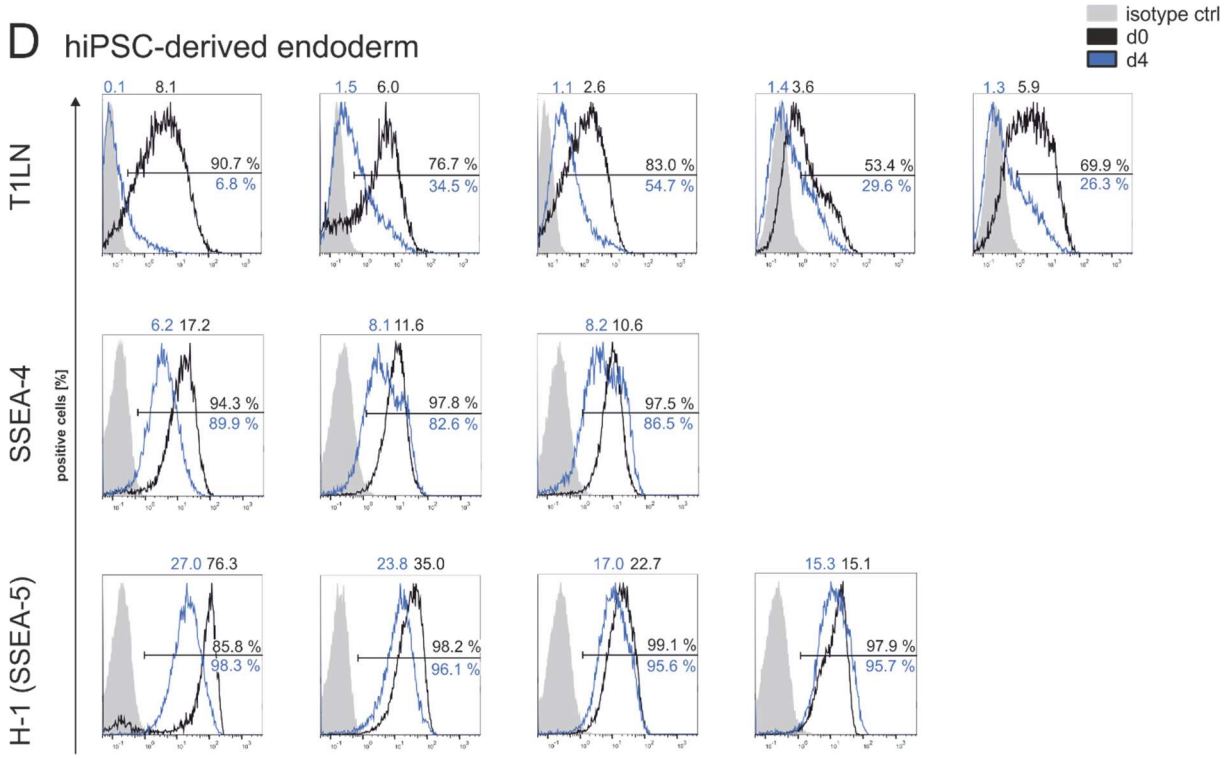
D hiPSC-derived endoderm
isotype ctrl
d0
d4
T1LN
SSEA-4
H-1 (SSEA-5)
positive cells [%]
0.1 8.1
90.7 %
6.8 %
1.5 6.0
76.7 %
34.5 %
1.1 2.6
83.0 %
54.7 %
1.4 3.6
53.4 %
29.6 %
1.3 5.9
69.9 %
26.3 %
6.2 17.2
94.3 %
89.9 %
8.1 11.6
97.8 %
82.6 %
8.2 10.6
97.5 %
86.5 %
27.0 76.3
85.8 %
98.3 %
23.8 35.0
98.2 %
96.1 %
17.0 22.7
99.1 %
95.6 %
15.3 15.1
97.9 %
95.7 %

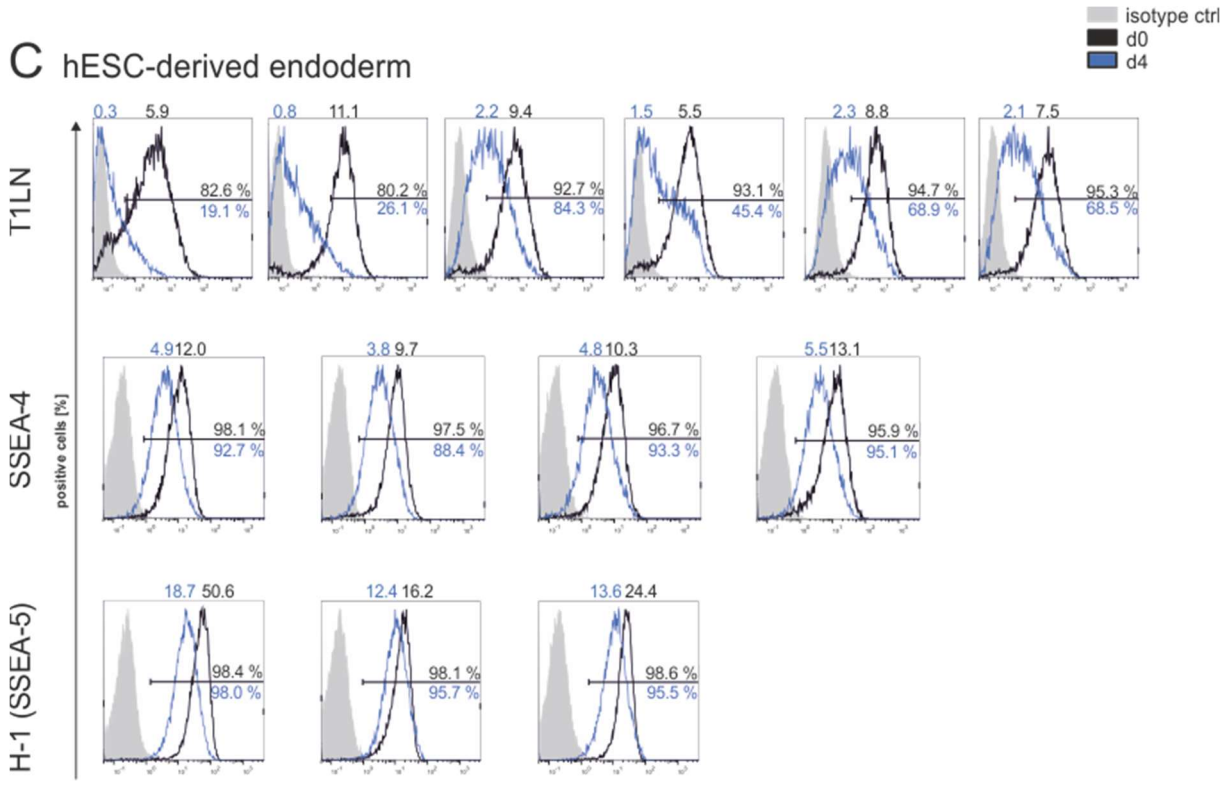
C hESC-derived endoderm
isotype ctrl
d0
d4
T1LN
SSEA-4
H-1 (SSEA-5)
positive cells [%]
0.3 5.9
82.6 %
19.1 %
0.8 11.1
80.2 %
26.1 %
2.2 9.4
92.7 %
84.3 %
1.5 5.5
93.1 %
45.4 %
2.3 8.8
94.7 %
68.9 %
2.1 7.5
95.3 %
68.5 %
4.9 12.0
98.1 %
92.7 %
3.8 9.7
97.5 %
88.4 %
4.8 10.3
96.7 %
93.3 %
5.5 13.1
95.9 %
95.1 %
18.7 50.6
98.4 %
98.0 %
12.4 16.2
98.1 %
95.7 %
13.6 24.4
98.6 %
95.5 %

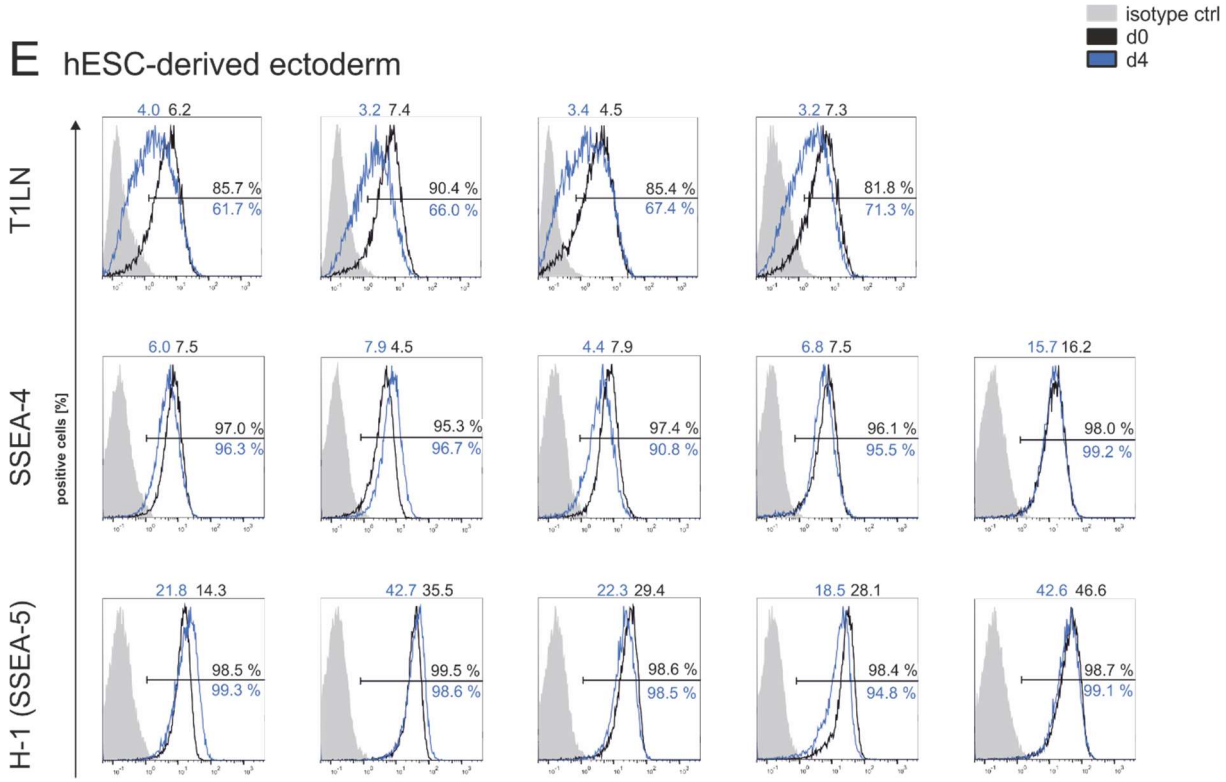
E hESC-derived ectoderm
isotype ctrl
d0
d4
T1LN
SSEA-4
H-1 (SSEA-5)
positive cells [%]
4.0 6.2
85.7 %
61.7 %
3.2 7.4
90.4 %
66.0 %
3.4 4.5
85.4 %
67.4 %
3.2 7.3
81.8 %
71.3 %
6.0 7.5
97.0 %
96.3 %
7.9 4.5
95.3 %
96.7 %
4.4 7.9
97.4 %
90.8 %
6.8 7.5
96.1 %
95.5 %
15.7 16.2
98.0 %
99.2 %
21.8 14.3
98.5 %
99.3 %
42.7 35.5
99.5 %
98.6 %
22.3 29.4
98.6 %
98.5 %
18.5 28.1
98.4 %
94.8 %
42.6 46.6
98.7 %
99.1 %

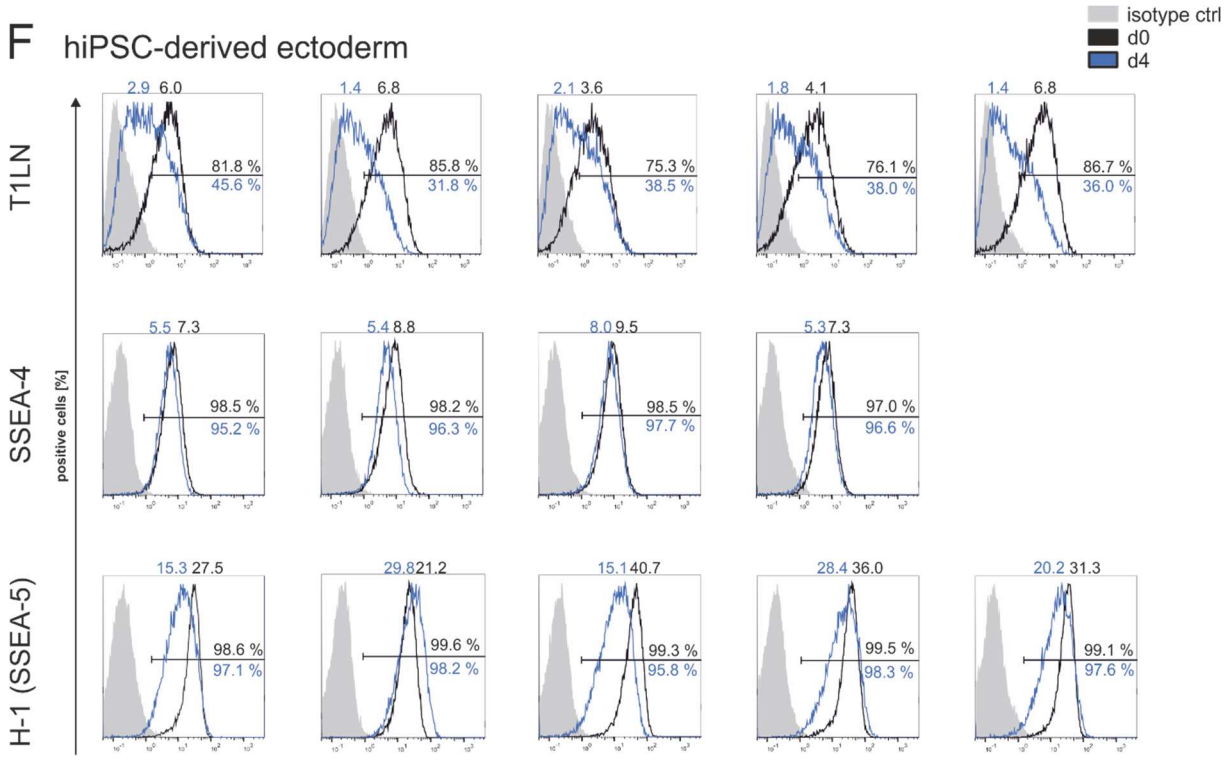
F hiPSC-derived ectoderm
isotype ctrl
d0
d4
T1LN
SSEA-4
H-1 (SSEA-5)
positive cells [%]
2.9 6.0
81.8 %
45.6 %
1.4 6.8
85.8 %
31.8 %
2.1 3.6
75.3 %
38.5 %
1.8 4.1
76.1 %
38.0 %
1.4 6.8
86.7 %
36.0 %
5.5 7.3
98.5 %
95.2 %
5.4 8.8
98.2 %
96.3 %
8.0 9.5
98.5 %
97.7 %
5.3 7.3
97.0 %
96.6 %
15.3 27.5
98.6 %
97.1 %
29.8 21.2
99.6 %
98.2 %
15.1 40.7
99.3 %
95.8 %
28.4 36.0
99.5 %
98.3 %
20.2 31.3
99.1 %
97.6 %

765 **Supplemental Figure 3. Cell surface expression of T1LN, SSEA-4, and SSEA-5 in**
766 **hPSCs and differentiated derivatives of all replicates shown in Figure 2**

767 (A-F) Flow cytometry analysis of hESC- (A) and hiPSC-derived mesoderm (B), hESC-
768 (C) and hiPSC-derived endoderm (D), and hESC- (E) and hiPSC-derived ectoderm (F)
769 on d0 and d4 of differentiation for T1LN (top), SSEA-4 (middle), and SSEA-5 (bottom).
770 Overlay histograms show fluorescence signal of viable cells on d0 (black) and d4
771 (blue). Cells were defined positive if the fluorescence signal was above that of 99 % of
772 the cells stained with the respective isotype control (grey). Only isotype controls for d0
773 are displayed but for calculation of positive cells on d4, isotype controls of d4 were
774 considered. Number of positive cells are shown below (blue) and above (black) the line
775 representing the gate. Mean fluorescence intensity is shown above histograms (d0,
776 black and d4, blue).

777

778

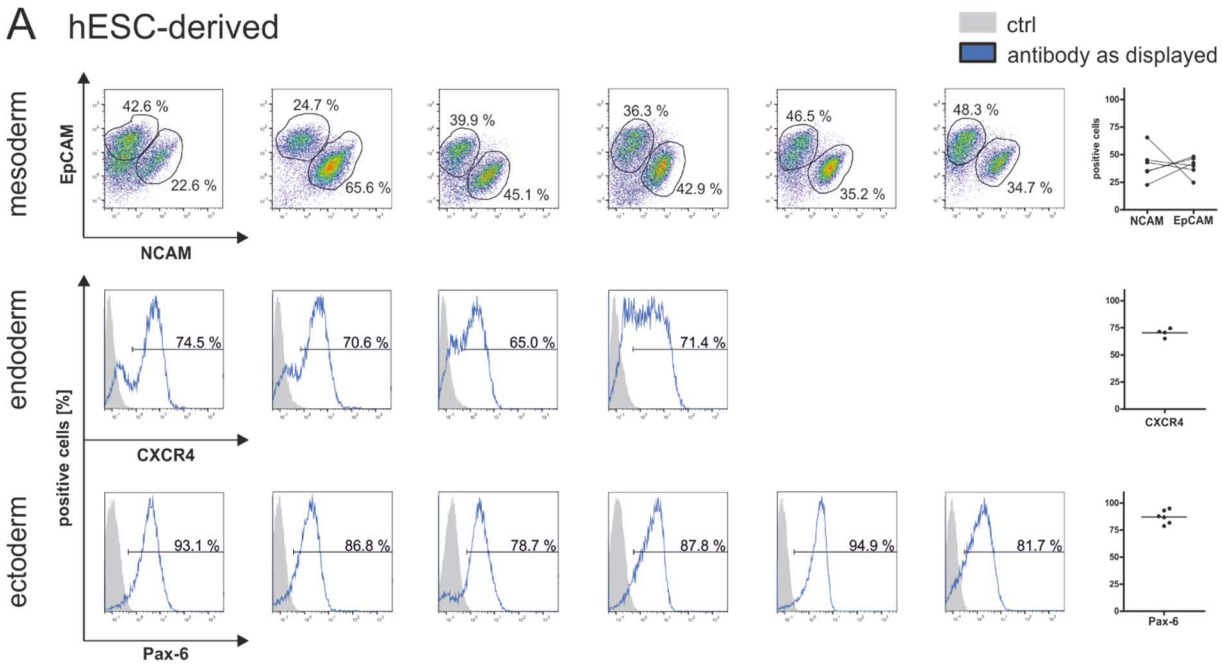
A hESC-derived
ctrl
antibody as displayed
mesoderm
EpCAM
NCAM
42.6 %
22.6 %
24.7 %
65.6 %
39.9 %
45.1 %
36.3 %
42.9 %
46.5 %
35.2 %
48.3 %
34.7 %
positive cells
NCAM EpCAM
endoderm
positive cells [%]
CXCR4
74.5 %
70.6 %
65.0 %
71.4 %
ectoderm
Pax-6
93.1 %
86.8 %
78.7 %
87.8 %
94.9 %
81.7 %

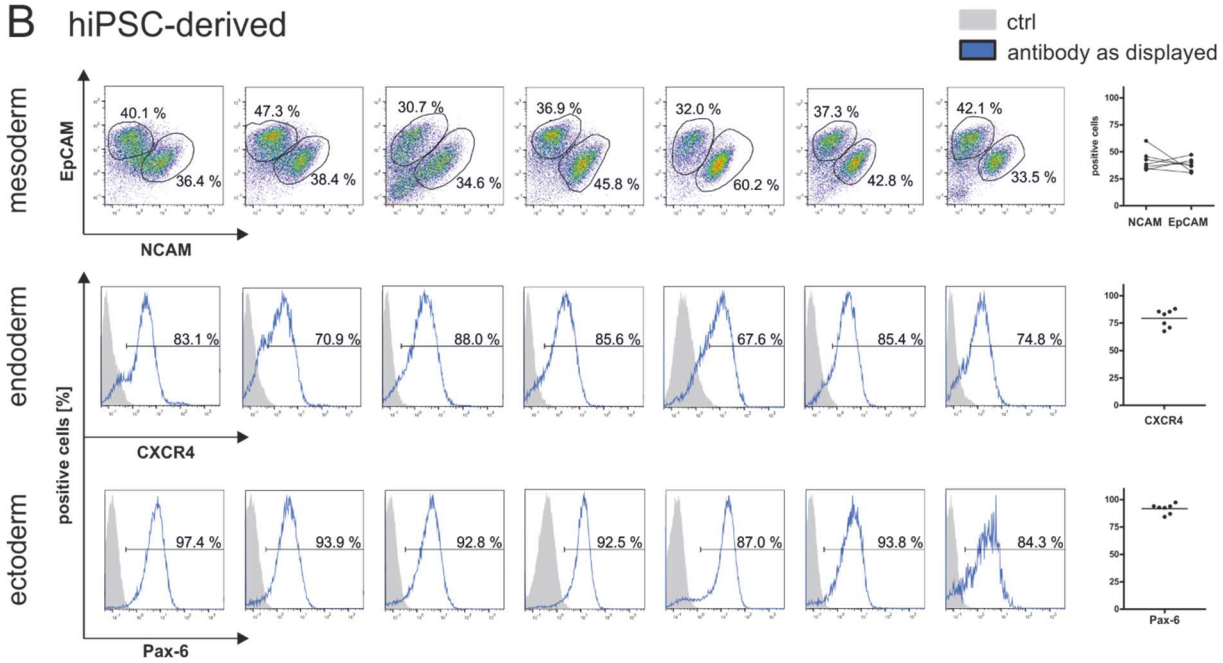
B hiPSC-derived
ctrl
antibody as displayed
mesoderm
EpCAM
NCAM
40.1 %
36.4 %
47.3 %
38.4 %
30.7 %
34.6 %
36.9 %
45.8 %
32.0 %
60.2 %
37.3 %
42.8 %
42.1 %
33.5 %
positive cells
NCAM EpCAM
endoderm
positive cells [%]
CXCR4
83.1 %
70.9 %
88.0 %
85.6 %
67.6 %
85.4 %
74.8 %
ectoderm
Pax-6
97.4 %
93.9 %
92.8 %
92.5 %
87.0 %
93.8 %
84.3 %

779

780

781 **Supplemental Figure 4. Quality control of differentiation approaches of**
782 **replicates shown in Figure 3**

783 (A-B) Differentiation of hESCs (A) and hiPSCs (B) into mesoderm (top panel),
784 endoderm (middle panel), and ectoderm (bottom panel) was confirmed by cell surface
785 staining of corresponding differentiation markers and quantified via flow cytometry. For
786 mesoderm, dot plots are displayed showing balanced NCAM and EpCAM expression
787 in viable cells on d4 of differentiation. For endoderm and ectoderm, overlay histograms
788 show fluorescence signal of viable cells on d4 of differentiation (blue) for CXCR4 and
789 Pax-6, respectively. Cells were defined positive if the fluorescence signal was above
790 that of 99 % of the cells stained with the respective control (ctrl, grey). Scatter plots
791 display all analyzed replicates shown in Figure 3.

A hESC-derived mesoderm
isotype ctrl
T1LN
d0
d4
d0/d4-pool
T1LN-pos
T1LN-neg
positive cells [%]
B hiPSC-derived mesoderm
isotype ctrl
T1LN
d0
d4
d0/d4-pool
T1LN-pos
T1LN-neg
positive cells [%]

792

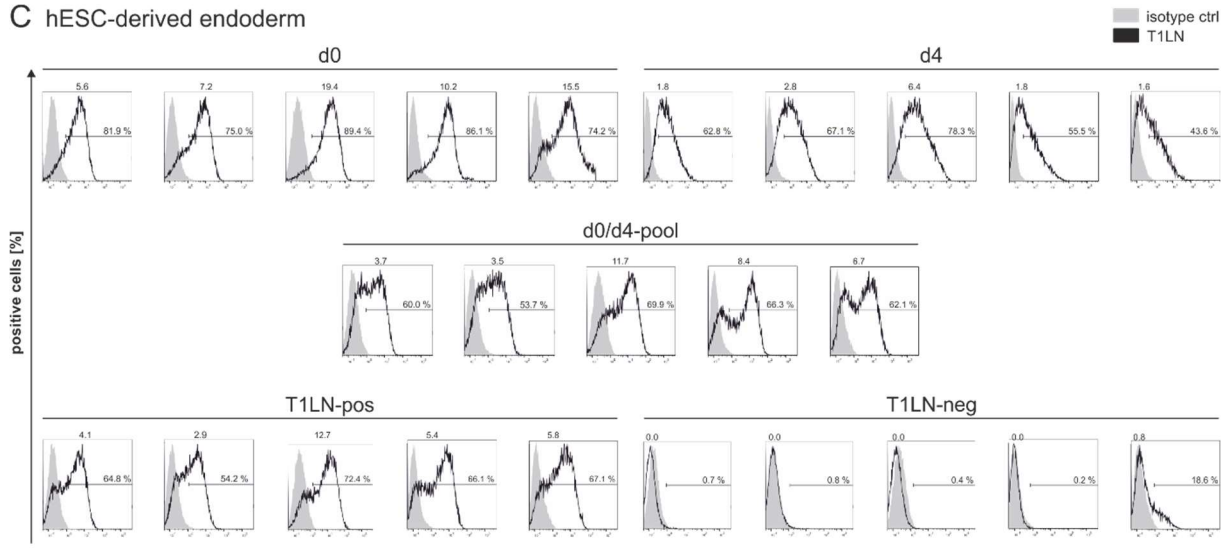
C hESC-derived endoderm
isotype ctrl
T1LN
d0
d4
d0/d4-pool
T1LN-pos
T1LN-neg
positive cells [%]
5.6
81.9 %
7.2
75.0 %
19.4
89.4 %
10.2
86.1 %
15.5
74.2 %
1.8
62.8 %
2.8
67.1 %
6.4
78.3 %
1.8
55.5 %
1.6
43.6 %
3.7
60.0 %
3.5
53.7 %
11.7
69.9 %
8.4
66.3 %
6.7
62.1 %
4.1
64.8 %
2.9
54.2 %
12.7
72.4 %
5.4
66.1 %
5.8
67.1 %
0.0
0.7 %
0.0
0.8 %
0.0
0.4 %
0.0
0.2 %
0.8
18.6 %

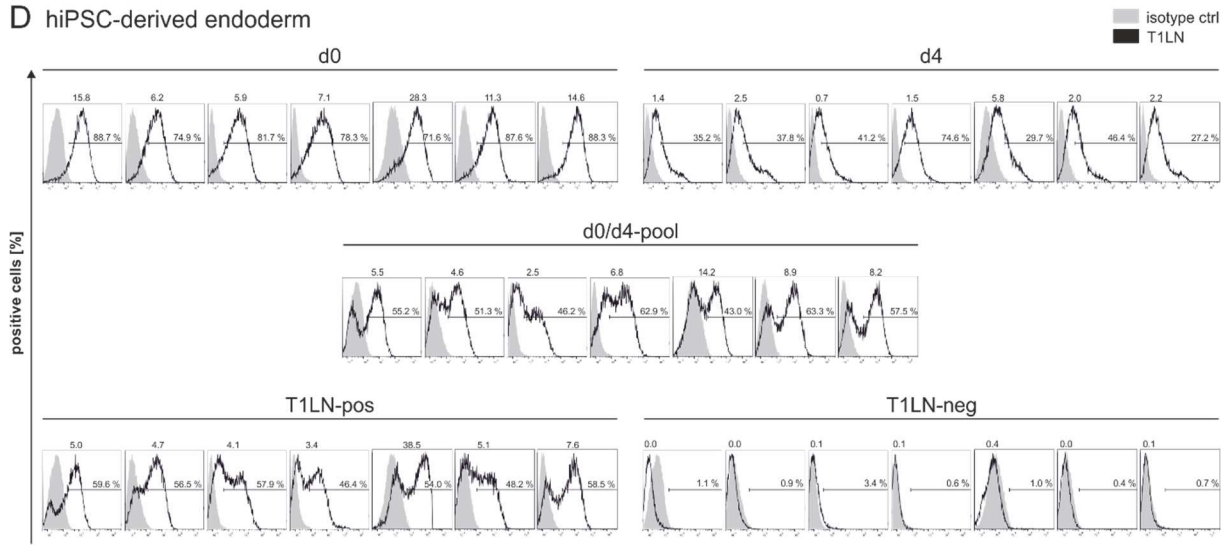
D hiPSC-derived endoderm
isotype ctrl
T1LN
d0
d4
d0/d4-pool
T1LN-pos
T1LN-neg
positive cells [%]
15.8
88.7 %
6.2
74.9 %
5.9
81.7 %
7.1
78.3 %
28.3
71.6 %
11.3
87.6 %
14.6
88.3 %
1.4
35.2 %
2.5
37.8 %
0.7
41.2 %
1.5
74.6 %
5.8
29.7 %
2.0
46.4 %
2.2
27.2 %
5.5
55.2 %
4.6
51.3 %
2.5
46.2 %
6.8
62.9 %
14.2
43.0 %
8.9
63.3 %
8.2
57.5 %
5.0
59.6 %
4.7
56.5 %
4.1
57.9 %
3.4
46.4 %
38.5
54.0 %
5.1
48.2 %
7.6
58.5 %
0.0
1.1 %
0.0
0.9 %
0.1
3.4 %
0.1
0.6 %
0.4
1.0 %
0.0
0.4 %
0.1
0.7 %

793

794

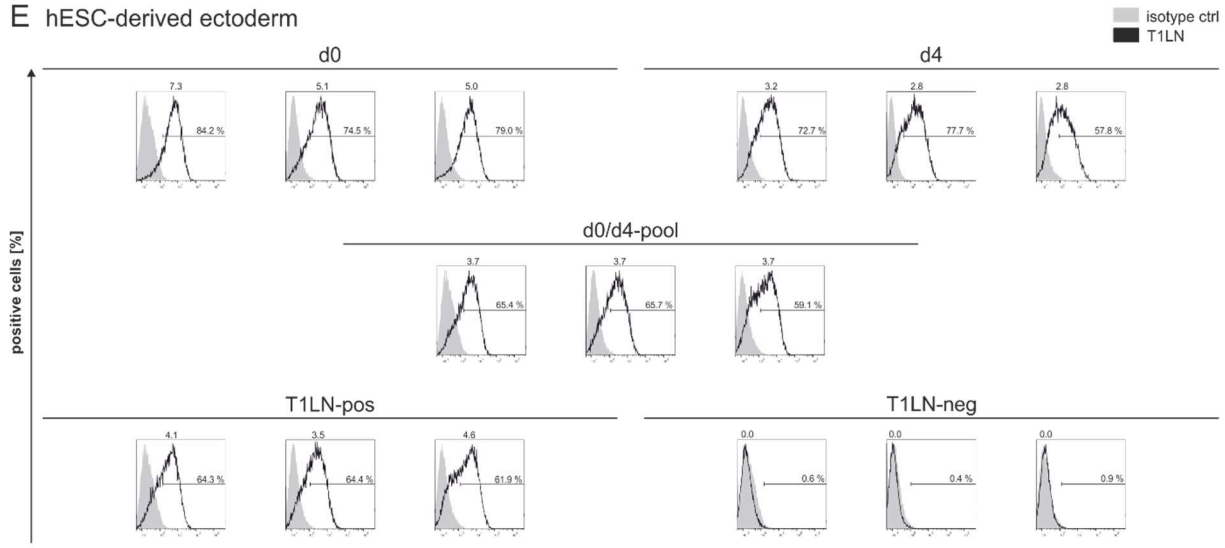
E hESC-derived ectoderm
isotype ctrl
T1LN
d0
d4
d0/d4-pool
T1LN-pos
T1LN-neg
positive cells [%]
7.3
84.2 %
5.1
74.5 %
5.0
79.0 %
3.2
72.7 %
2.8
77.7 %
2.8
57.8 %
3.7
65.4 %
3.7
65.7 %
3.7
59.1 %
4.1
64.3 %
3.5
64.4 %
4.6
61.9 %
0.0
0.6 %
0.0
0.4 %
0.0
0.9 %

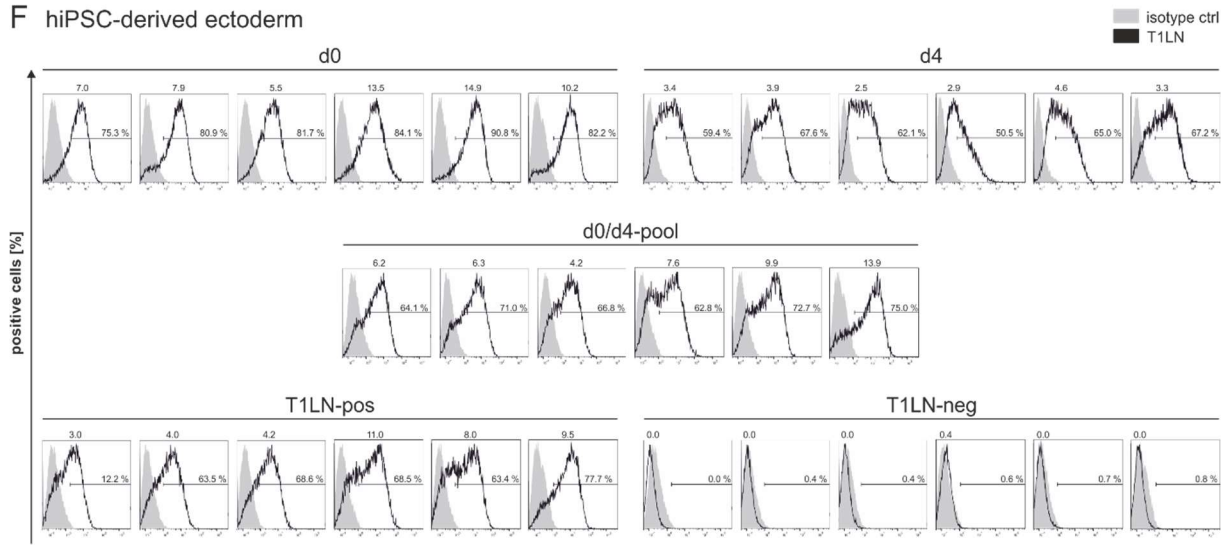
F hiPSC-derived ectoderm
isotype ctrl
T1LN
d0
d4
d0/d4-pool
T1LN-pos
T1LN-neg
positive cells [%]
7.0
75.3 %
7.9
80.9 %
5.5
81.7 %
13.5
84.1 %
14.9
90.8 %
10.2
82.2 %
3.4
59.4 %
3.9
67.6 %
2.5
62.1 %
2.9
50.5 %
4.6
65.0 %
3.3
67.2 %
6.2
64.1 %
6.3
71.0 %
4.2
66.8 %
7.6
62.8 %
9.9
72.7 %
13.9
75.0 %
3.0
12.2 %
4.0
63.5 %
4.2
68.6 %
11.0
68.5 %
8.0
63.4 %
9.5
77.7 %
0.0
0.0 %
0.0
0.4 %
0.0
0.4 %
0.4
0.6 %
0.0
0.7 %
0.0
0.8 %

795

796

797 **Supplemental Figure 5. Cell surface expression of T1LN in hPSCs and**
798 **differentiated derivatives pre- and post-MACS of all replicates shown in Figure 3**

799 (A-E) Cell surface expression was analyzed using flow cytometry pre-MACS in d0 (top
800 left), d4 (top right) and d0/d4-pooled cells (middle), as well as post-MACS in the T1LN-
801 positive (bottom left) and T1LN-negative population (bottom right) in hESC- (A) and
802 hiPSC-derived mesoderm (B), hESC- (C) and hiPSC-derived endoderm (D), and
803 hESC- (E) and hiPSC-derived ectoderm (F). Overlay histograms show fluorescence
804 signal of viable cells (black) in regard to the respective isotype control (isotype ctrl,
805 shown in grey). Cells were defined positive if the fluorescence signal was above that
806 of 99 % of the cells stained with the respective isotype control. Only isotype controls
807 for d0 are displayed, but for calculation of positive cells on d4 isotype controls of d4
808 were considered. For calculation of positive cells post-MACS, both isotype controls of
809 d0 and d4 were considered. Number of positive cells are shown above the line
810 representing the gate. Mean fluorescence intensity is shown above histograms.

811

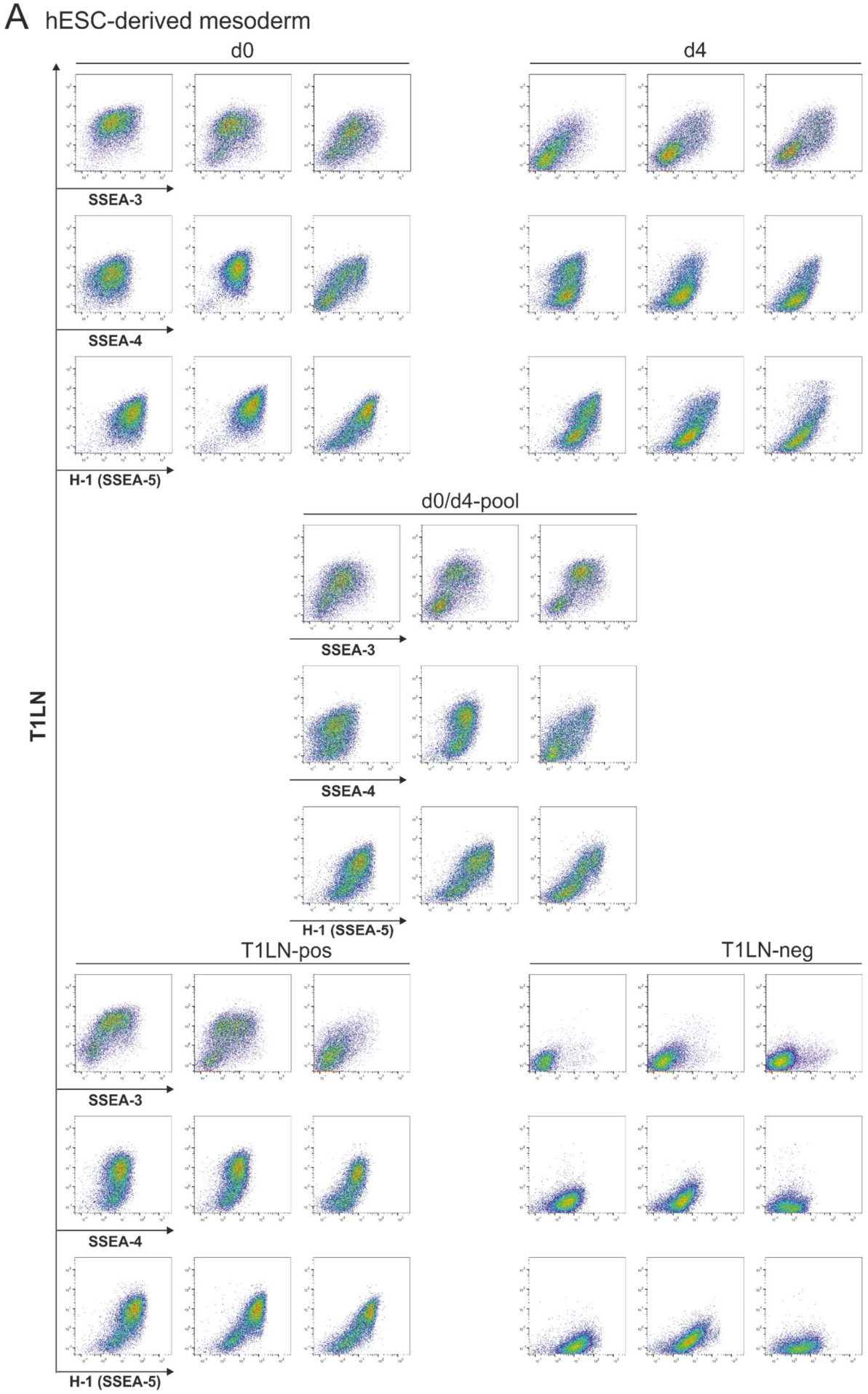
A hESC-derived mesoderm
d0
d4
d0/d4-pool
T1LN-pos
T1LN-neg
T1LN
SSEA-3
SSEA-4
H-1 (SSEA-5)

812

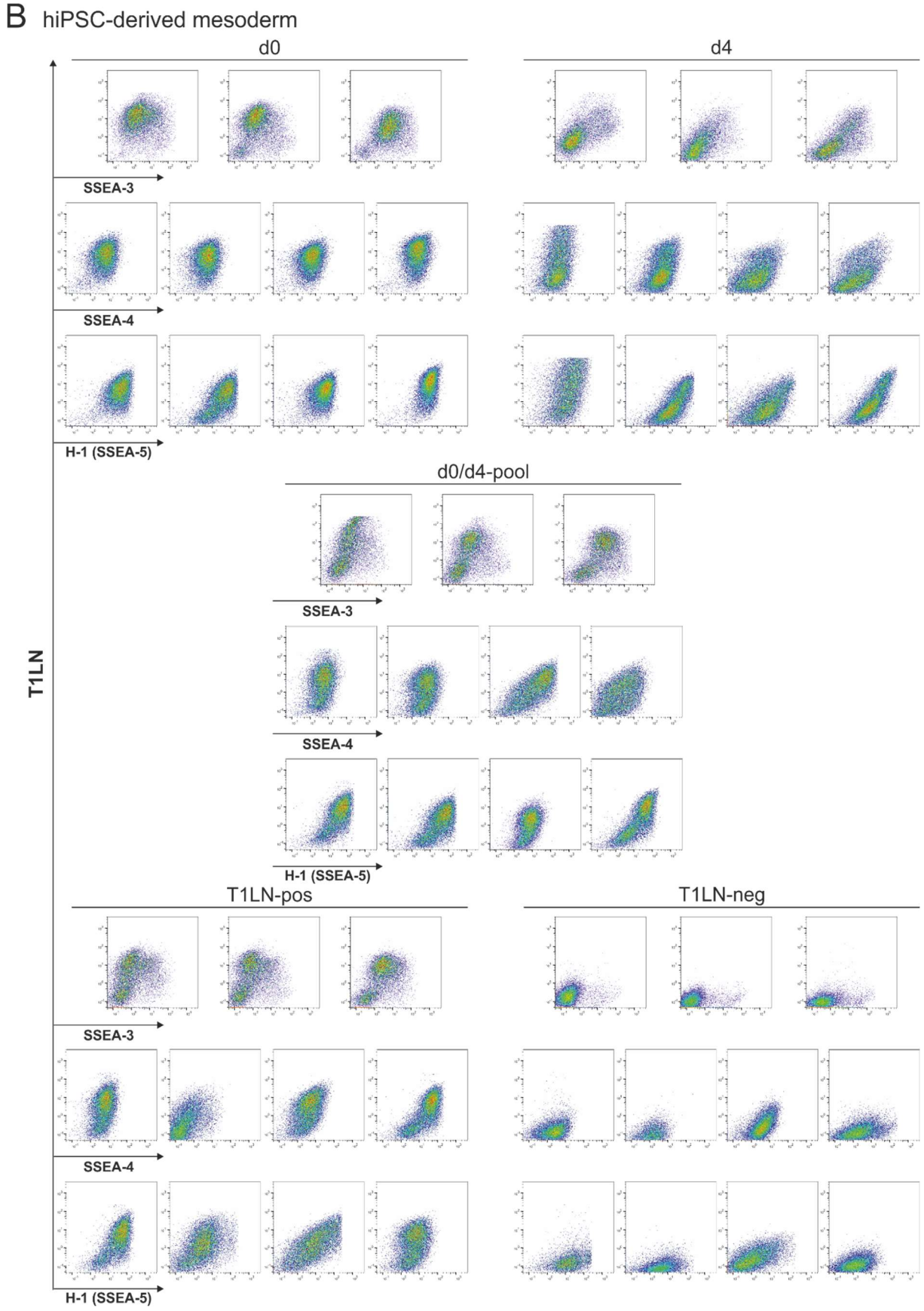
B hiPSC-derived mesoderm
d0
d4
d0/d4-pool
T1LN-pos
T1LN-neg
T1LN
SSEA-3
SSEA-4
H-1 (SSEA-5)

813

C hESC-derived endoderm

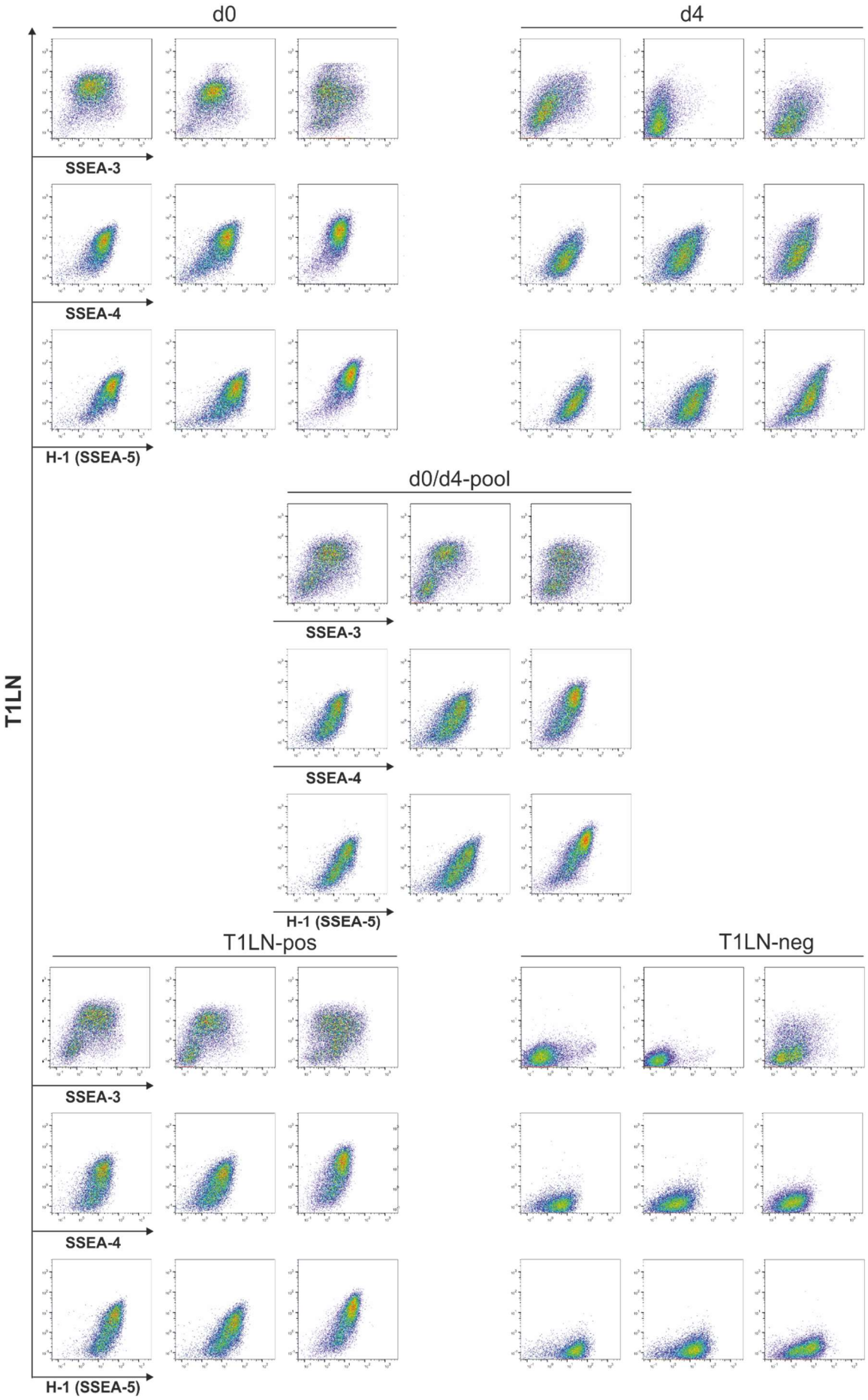

814

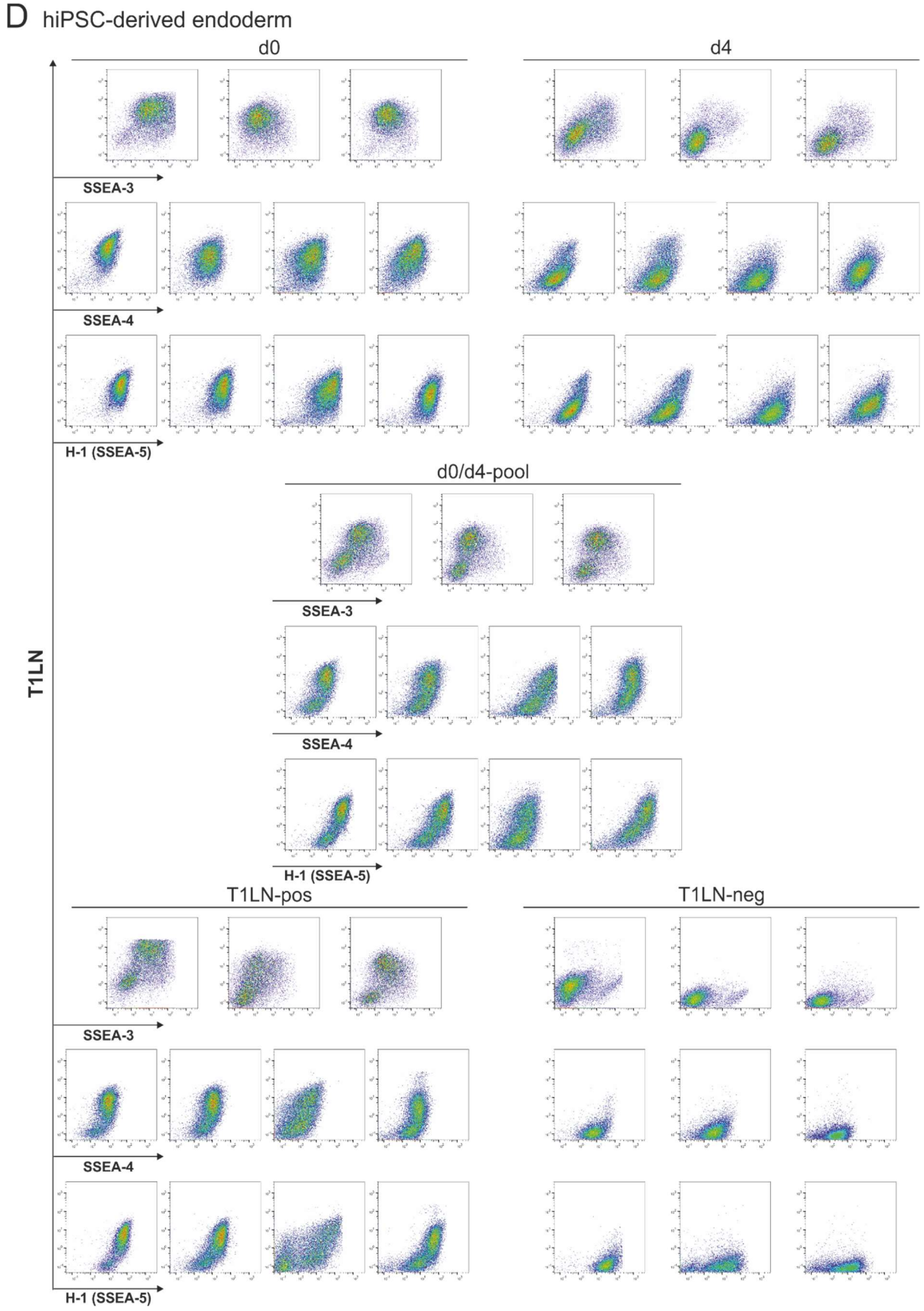
D hiPSC-derived endoderm
d0
d4
d0/d4-pool
T1LN-pos
T1LN-neg
T1LN
SSEA-3
SSEA-4
H-1 (SSEA-5)

815

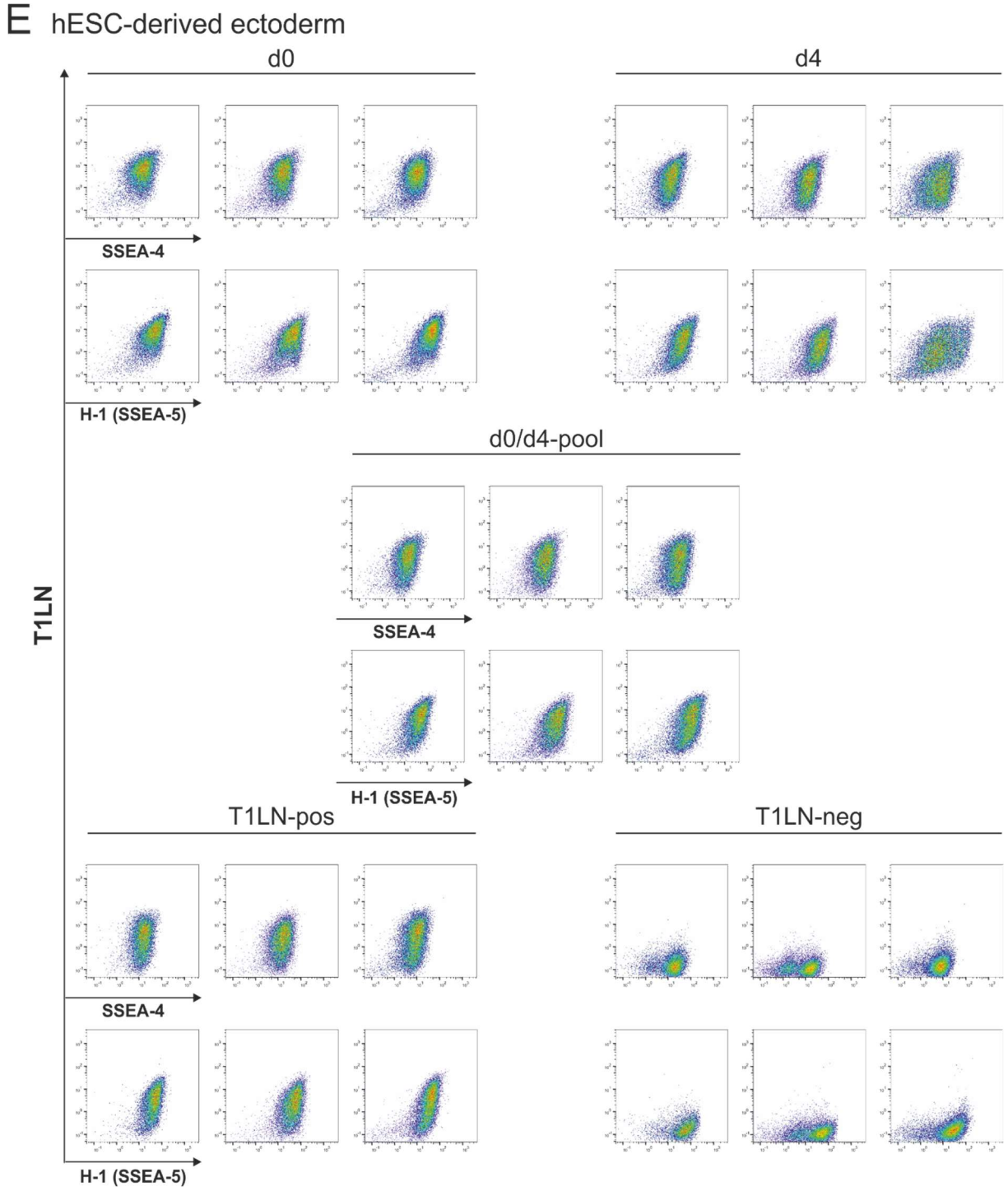
E
hESC-derived ectoderm
d0
d4
SSEA-4
H-1 (SSEA-5)
d0/d4-pool
SSEA-4
H-1 (SSEA-5)
T1LN
T1LN-pos
T1LN-neg
SSEA-4
H-1 (SSEA-5)

816

F hiPSC-derived ectoderm

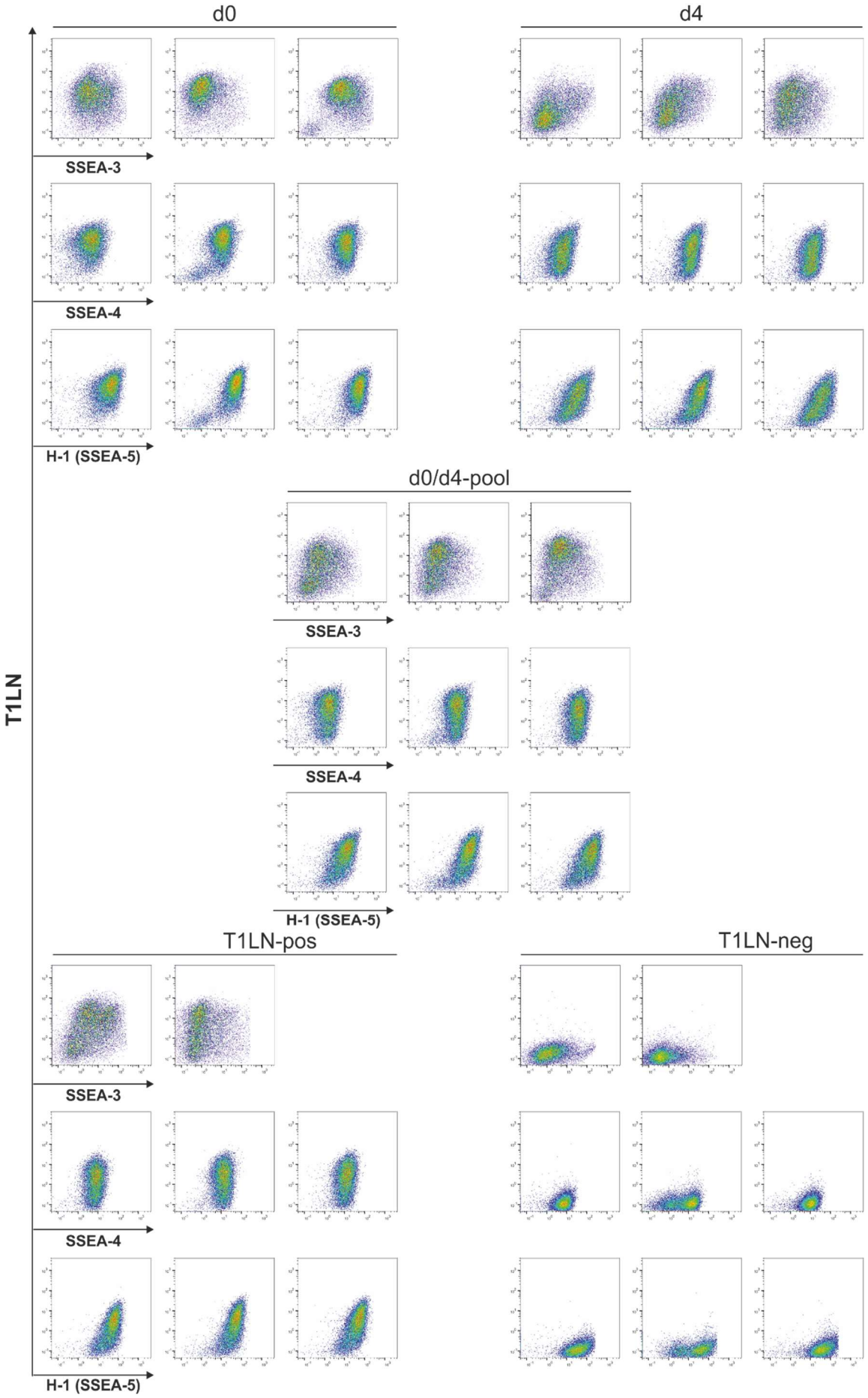

817

818 **Supplemental Figure 6. Cell surface expression of T1LN, SSEA-3, SSEA-4, and**
819 **SSEA-5 in hPSCs and differentiated derivatives pre- and post-MACS of all**
820 **replicates shown in Figure 3**

821 (A-F) Cell surface expression was analyzed using flow cytometry pre-MACS in d0 (top
822 left), d4 (top right) and d0/d4-pooled cells (middle), as well as post-MACS in the T1LN-
823 positive (bottom left) and T1LN-negative population (bottom right) in hESC- (A) and
824 hiPSC-derived mesoderm (B), hESC- (C) and hiPSC-derived endoderm (D), and
825 hESC- (E) and hiPSC-derived ectoderm (F). Dot plots display cell surface expression
826 of T1LN and SSEA-3 (top panel), Lc4 and SSEA-4 (middle panel), as well as cell
827 surface expression of T1LN and SSEA-5 (bottom panel).